Geosci. Model Dev., 17, 4311–4330, 2024
https://doi.org/10.5194/gmd-17-4311-2024

Geoscientific Model Development
Open Access
EGU

Development of a multiphase chemical mechanism to improve secondary organic aerosol formation in CAABA/MECCA (version 4.7.0)

Felix Wieser[1], Rolf Sander[2], Changmin Cho[1,a], Hendrik Fuchs[1,3], Thorsten Hohaus[1], Anna Novelli[1], Ralf Tillmann[1], and Domenico Taraborrelli[1]

[1]Institute of Energy and Climate Research, IEK-8: Troposphere, Forschungszentrum Jülich GmbH, Jülich, Germany
[2]Atmospheric Chemistry Department, Max Planck Institute for Chemistry, Mainz, Germany
[3]Department of Physics, University of Cologne, Cologne, Germany
[a]now at: Atmospheric Chemistry Observations and Modeling Laboratory, National Center for Atmospheric Research, Boulder, CO, USA

Correspondence: Felix Wieser (f.wieser@fz-juelich.de) and Domenico Taraborrelli (d.taraborrelli@fz-juelich.de)

Received: 23 May 2023 – Discussion started: 26 May 2023
Revised: 21 March 2024 – Accepted: 3 April 2024 – Published: 24 May 2024

Abstract. During the last few decades, the impact of multiphase chemistry on secondary organic aerosols (SOAs) has been demonstrated to be the key to explaining laboratory experiments and field measurements. However, global atmospheric models still show large biases when simulating atmospheric observations of organic aerosols (OAs). Major reasons for the model errors are the use of simplified chemistry schemes of the gas-phase oxidation of vapours and the parameterization of heterogeneous surface reactions. The photochemical oxidation of anthropogenic and biogenic volatile organic compounds (VOCs) leads to products that either produce new SOA or are taken up by existing aqueous media like cloud droplets and deliquescent aerosols. After partitioning, aqueous-phase processing results in polyols, organosulfates, and other products with a high molar mass and oxygen content. In this work, we introduce the formation of new low-volatility organic compounds (LVOCs) to the multiphase chemistry box model CAABA/MECCA. Most notable are the additions of the SOA precursors, limonene and *n*-alkanes (5 to 8 C atoms), and a semi-explicit chemical mechanism for the formation of LVOCs from isoprene oxidation in the gas and aqueous phases. Moreover, Henry's law solubility constants and their temperature dependences are estimated for the partitioning of organic molecules to the aqueous phase. Box model simulations indicate that the new chemical scheme predicts the enhanced formation of LVOCs, which are known for being precursor species to SOAs. As expected, the model predicts that LVOCs are positively correlated to temperature but negatively correlated to NO_x levels. However, the aqueous-phase processing of isoprene epoxydiols (IEPOX) displays a more complex dependence on these two key variables. Semi-quantitative comparison with observations from the SOAS campaign suggests that the model may overestimate methylbutane-1,2,3,4-tetrol (MeBuTETROL) from IEPOX. Further application of the mechanism in the modelling of two chamber experiments, one in which limonene is consumed by ozone and one in which isoprene is consumed by NO_3 shows a sufficient agreement with experimental results within model limitations. The extensions in CAABA/MECCA are transferred to the 3D atmospheric model MESSy for a comprehensive evaluation of the impact of aqueous- and/or aerosol-phase chemistry on SOA at a global scale in a follow-up study.

1 Introduction

Secondary organic aerosol (SOA) is formed from anthropogenic and biogenic volatile organic compounds (VOCs) in the atmosphere and comprises a significant portion of the total organic aerosol (OA) mass (Hallquist et al., 2009). Atmospheric aerosols have received increased attention in recent years as a result of their impact on human health, urban visi-

bility, and climate change (Zhong and Jang, 2011; Zhu et al., 2017; Lin et al., 2017; Chen et al., 2020). New SOA precursors, formation pathways, and loss reactions in the gas and the aqueous phase have been discovered (Lim et al., 2010; Hodzic et al., 2014; Wennberg et al., 2018). In current models, aqueous-phase pathways leading to SOA continuously improve, as their importance has been demonstrated in experiments (Carlton et al., 2007; Lin et al., 2014; Ervens, 2015). Hu et al. (2015) investigated aqueous SOA (aqSOA) tracers from isoprene oxidation and found a contribution between 6 % and 36 % to total OA.

Recent models show different biases in their results. Traditional global models generally underestimate SOA mass, especially during haze events, due to the increase in pollutant concentrations (Heald et al., 2011; Tilmes et al., 2019). This gap between models and observations has been continuously decreasing in recent years, but SOA formed in the available aqueous phase is often still neglected (Shrivastava et al., 2017). Aqueous SOA is known to be more oxidized than SOA formed from gas-phase precursors; thus, the modelled O / C ratios commonly do not match experimental results (Lim et al., 2010). Additionally, products from aqueous-phase oxidation are formed in different timescales than from gas-phase oxidation. Combined with aqueous- and gas-phase properties (pollutants and pH), this impacts the vertical distribution of SOA in the atmosphere depending on the simulation setup (Seinfeld and Pandis, 2016; Hodzic et al., 2016).

We have implemented recent experimental results and formerly neglected SOA precursors into the chemistry scheme of the box model CAABA/MECCA. The updated chemical mechanism is meant to be used to further advance global simulations of SOA with the EMAC (ECHAM/MESSy Atmospheric Chemistry) model (Pozzer et al., 2022). EMAC is the global configuration of the Modular Earth Submodel System (MESSy) (Jöckel et al., 2006; Tost et al., 2006; Kerkweg et al., 2007; Jöckel et al., 2010, 2016). This approach has two advantages: (1) model simulations in the test phase are considerably faster in the box than in the global model and (2) thanks to the MESSy interface structure, the MECCA chemical mechanism can directly be used in the global model EMAC. This allows us to be fast with the implementation process, while being able to use the new chemistry in the global model without further adaptations. The partitioning to the from aqueous to particle phases plays an important role in the SOA formation process. As temperature-dependent Henry's law solubility constants (H_s) for large organic molecules are sparse in the literature, these properties have to be estimated. The corresponding approach is discussed in Sect. 2.4. In Sect. 3, the new chemical scheme is evaluate against model, observational, and chamber data. In the following section, we introduce the major specifications of the CAABA/MECCA model.

2 Model description

2.1 Specifications

CAABA/MECCA is a combination of the box model CAABA (Chemistry As A Box model Application) and the atmospheric chemistry model MECCA (Module Efficiently Calculating the Chemistry of the Atmosphere) (Sander et al., 2019). The chemistry module MECCA is also used in the global model EMAC, simplifying the adoption of box model changes into the global model. MECCA contains both gas- and aqueous-phase chemistry, and the species can partition between the phases. Simulations with solely the gas phase are also possible to simulate dry conditions. For the partitioning, Henry's law solubility constants are utilized. Non-linear effects like "salting in" and "salting out" influence Henry's law solubility constants. It has been shown that the partitioning of compounds can be substantially influenced by the aerosol salt concentration (Kampf et al., 2013; Herrmann et al., 2015). Similarly, aqueous-phase reaction rates can be influenced by salt composition (Mekic and Gligorovski, 2021). The model does not account for these effects due to the insufficient data availability (Sander, 2023). This may result in partially incorrect partitioning rates.

Available mechanisms for organic chemistry are the Mainz Organic Mechanism (MOM) (Sander et al., 2019) and the Jülich Aqueous-phase Mechanism of Organic Chemistry (JAMOC) by Rosanka et al. (2021). MOM is the default oxidation mechanism of VOCs in MECCA. It contains an advanced treatment of chemistry of isoprene (Taraborrelli et al., 2012; Nölscher et al., 2014; Novelli et al., 2020), monoterpenes (Hens et al., 2014; Mallik et al., 2018), and aromatics (Cabrera-Perez et al., 2016; Taraborrelli et al., 2021). JAMOC is a reduced subset of the CLEPS mechanism (Mouchel-Vallon et al., 2017). Although built for global chemistry simulations, the two chemical mechanisms together cover a wide range of reactions. When combined, they include gas-phase oxidation and gas-to-aqueous-phase partitioning for species with up to 11 carbons and aqueous-phase oxidation for species with up to 4 carbons. The submodel JVAL calculates photochemical rate constants (j values) based on cross sections and quantum yields (Sander et al., 2014). The related j values are usually first determined for the smallest compound of a compound class, and this value is applied to higher homologs. For instance, j values for the photolysis of all organic hydroperoxides are taken to be equal to the one for methyl hydroperoxide (j_{CH_3OOH}). This is also done in the Master Chemical Mechanism (MCM) (Jenkin et al., 1997). More details about CAABA/MECCA can be found elsewhere (Sander et al., 2005, 2011, 2019).

2.2 Model limitations

The main goal of the CAABA/MECCA box model is the investigation of chemical reaction mechanisms in the atmo-

sphere. Other processes (e.g. dynamics and microphysics) are simplified or neglected. Specifically, the formation and loss of SOA are not included. Cloud droplets and rain were not modelled and, therefore, neither was scavenging or wet deposition. Low-volatility organic compounds (LVOCs) can dissolve and react in deliquescent (aqueous) aerosols but not in an organic apolar medium. We chose CAABA/MECCA regardless of the mentioned limitations, as this study is intended to present the chemistry scheme and demonstrate the possible influence of the update on future results. We applied the following assumptions to display the ability of the chemical mechanism to simulate experimental and/or observational results. Generally, we assume LVOCs as a proxy for SOAs, disregarding the partitioning process. To model the isoprene observation, LVOCs are defined as compounds that exhibit an H_s larger than $10^8\,\mathrm{M\,atm^{-1}}$ (see Sect. 3.1.2). For the experiment in which limonene is consumed by ozone, a lower H_s threshold of $4 \times 10^6\,\mathrm{M\,atm^{-1}}$ was selected. This rule is applied to species in the gas phase and the aqueous phase to tackle the missing condensation and new particle formation. Different thresholds were chosen due to varying conditions affecting the importance of condensation and new particle formation and the molar mass of the major SOA products. Limonene products are more likely to condense on preexisting aerosols due to their lower saturation vapour pressure. We intend to give an advanced evaluation of the presented mechanisms in the global model EMAC with a mechanism that is extended further. Due to the wide range of available submodules solving most of the abovementioned limitations (Tost et al., 2006; Pringle et al., 2010; Tsimpidi et al., 2014; Ehrhart et al., 2018), EMAC can give a more in-depth analysis of the impact of the mechanism and advances needed in future updates.

2.3 Mechanism development

2.3.1 Overview

Table 1 lists the newly implemented and updated precursors split into biogenic and anthropogenic origin. A major update to the chemical mechanism is introduced by updating the isoprene oxidation scheme. Additionally, the β-pinene and benzene mechanisms were revised. Limonene, IEPOX, and n-alkane mechanisms were newly added. The chemistry schemes of the monoterpenes sabinene, camphene, and carene were based on α-pinene and were not developed for the individual compounds. They are currently excluded as they do not fulfil the standard of the implemented chemistry and will potentially be reintroduced with a more refined mechanism. The impact of these monoterpenes on LVOCs in the forward analysis is small, as depicted in Fig. S9 in the Supplement. In the following sections, changes to the specific mechanisms are described in detail.

2.3.2 Gas-phase kinetics

The addition of a nitrate radical to isoprene is improved on based on Vereecken et al. (2021), which has been validated against chamber experiments (Carlsson et al., 2023). The former oxidation mechanism in MECCA is substituted by new pathways and products, including epoxide formation. The resulting mechanism represents a subset of the original scheme by Vereecken et al. (2021). Isoprene OH oxidation under low-NO_x conditions is revised by adding the formation of epoxydiol (IEPOX) according to St. Clair et al. (2016) and dihydroxy hydroperoxy epoxide (ISOPBEPX) according to D'Ambro et al. (2017). Both compounds were previously identified as the main SOA precursors (Lopez-Hilfiker et al., 2016; D'Ambro et al., 2017). Furthermore, the gas-phase oxidation of IEPOX, as described by Bates et al. (2014), is included in the new mechanism. The monoterpenes α-pinene and β-pinene are already included in the MECCA scheme with a refined mechanism. To simulate a wide range of monoterpenes, the oxidation of limonene was added to the model. The update is based on the chemical scheme of the Master Chemical Mechanism (MCM v3.3.1) by Jenkin et al. (1997) (http://mcm.york.ac.uk, last access: 13 May 2024). If available, reaction rates are re-calculated by structure–activity relationships (SARs), and low-yield pathways are excluded. Furthermore, the mechanism was refined by the results of Carslaw (2013) and Vereecken and Peeters (2012). Branching ratios of the mechanism of limonene and ozone were adapted by Pang et al. (2022). Products important to SOA are highly oxidized large hydroperoxides and ketones. Small adjustments referring to Vereecken and Peeters (2012) were introduced for β-pinene.

Anthropogenic SOA precursors are represented by aromatics and n-alkanes. The oxidation scheme of benzene and toluene is rather detailed in the model, while higher substituted aromatics are treated in a simplified manner (Cabrera-Perez et al., 2016; Taraborrelli et al., 2021). Benzene chemistry is updated according to the results by Xu et al. (2020), who found no evidence for the epoxide channel. This was validated by previous theoretical work by Vereecken (2019). We distribute the epoxide production into competing pathways (see Fig. S7). This adaptation yields more small, oxidized compounds like glyoxal. Thus, a decrease in SOA mass in the absence of cloud processing and efficient oligomer formation is expected. Similar changes for the epoxide channel were found for the OH oxidation of toluene, but, at the same time, the formation of alternate epoxides was shown (Wu et al., 2014; Zaytsev et al., 2019). The MOM treats the oxidation of alkanes with up to four carbons. Based on the field measurements of McDonald et al. (2018), the mechanism has been extended for n-alkanes with sizable emissions (up to n-octane). The n-alkane mechanism is based on the work of Atkinson et al. (2008) and yields hydroperoxides, alkyl nitrates, and organic molecules containing ketone and hydroxyl groups. This mechanism is simplified and thus only

Table 1. List of all newly implemented and updated VOC, together with the main reactants and main mechanism sources. Compounds are divided into biogenic and anthropogenic origin.

Precursor	Implementation type	Main reactant	Mechanism sources
Biogenic			
Isoprene	update	NO_3	Vereecken et al. (2021)
Isoprene	update	OH	St. Clair et al. (2016), Bates et al. (2014) D'Ambro et al. (2017)
IEPOX	new	OH	Petters et al. (2021), Riedel et al. (2016)
Limonene	new	OH/ozone/NO_3	MCM, Pang et al. (2022), Carslaw (2013), Vereecken and Peeters (2012)
β-Pinene	update	OH	Vereecken and Peeters (2012)
Sabinene/carene/camphene	excluded	OH/ozone	
Anthropogenic			
Benzene	update	OH	Xu et al. (2020), Wang et al. (2013)
Pentane, hexane	new	OH	Sivaramakrishnan and Michael (2009)
Heptane, octane			Atkinson et al. (2008)

covers the oxidation of specific reaction sites, and only one H abstraction process is considered.

Experimental studies have shown the partitioning of multifunctional alkyl nitrates to the aerosol phase (Perring et al., 2013). The yields of alkyl nitrates from the new $RO_2 + NO$ reactions for limonene and n-alkanes are implemented following the protocol by Sander et al. (2019). These yields depend on the number of heavy atoms, temperature, and pressure (Arey et al., 2001; Teng et al., 2015). Thus, the updated model is expected to generate significant amounts of SOA precursors over continental polluted regions during wintertime.

The rate constants for common reactions (e.g. OH addition and H abstraction) are taken from predefined functions implemented in MECCA, while rate constants for specific reactions are taken from the literature or are calculated by the SAR (Kwok and Atkinson, 1995; Sander et al., 2019). In the isoprene and limonene mechanisms, we consider H shifts in peroxy radicals, as described and estimated by Vereecken and Nozière (2020). In this scheme, the H shift depends on neighbouring substituents, yielding mainly highly oxygenated molecules (HOMs). New hydroperoxides either react with OH radicals by H abstraction to reform the corresponding peroxy radical or decompose into an alkoxy and an OH radical. The decomposition step mainly applies to molecules with neighbouring reactive groups, e.g. double bonds, which show a high reactivity towards alkoxy radicals, yielding epoxides. This kinetic scheme is key to IEPOX and ISOPBEPX formation. In the alkane oxidation mechanism, alkoxy radicals mainly undergo 1,5 H shifts. Graphical representations of the main pathways of all new reaction mechanisms are shown in Figs. S1–S8 in the Supplement.

2.3.3 Aqueous-phase kinetics

Rate constants and branching ratios in the aqueous phase are taken from Mouchel-Vallon et al. (2017) if available. Similar to the CLEPS 1.0 protocol, H abstractions by hydroxyl radicals are estimated with the SAR by Monod and Doussin (2008). Only the fastest H-abstraction pathways are considered, even though the SAR provides branching ratios for the different reactive sites. The examination of all CH bonds would require a general aqueous-phase C–H abstraction scheme in MECCA for all generated products, which is not included in the present model.

The kinetics of the IEPOX reactive uptake (acid-catalysed ring opening) are taken from the supplementary information of Petters et al. (2021), while the branching ratios are extracted from Riedel et al. (2016). In a moderately polluted atmosphere, methylbutane-1,2,3,4-tetrol (MeBuTETROL) is the main product of aqueous IEPOX oxidation, while the corresponding organosulfate is dominant in the presence of sulfate aerosols. As an addition to the production scheme, we developed and implemented a loss mechanism based on Cope et al. (2021), which we similarly applied to ISOPBEPX. Cope et al. (2021) revealed formic acid as the main oxidation product. They proposed a mechanism, explaining the formic acid formation, invoking some reactions to proceed at unusual rates in aqueous media. Figure 1 shows our adapted and revised mechanism. Comparing the typical rate constants of the possible pathways, we redistributed the oxygen abstraction by NO to the HO_2 elimination. The latter is, nevertheless, consistent with the observed formic acid yield. Similar to the mechanism by Cope et al. (2021), Fig. 1 displays the abstraction of the hydrogen atom at C_4 in the mechanism. In addition, we implemented the abstraction of the hydrogen atom at C_1 after the HO_2 elimination, yielding hydroxyacetone (not shown). Oxidation of the latter leads to

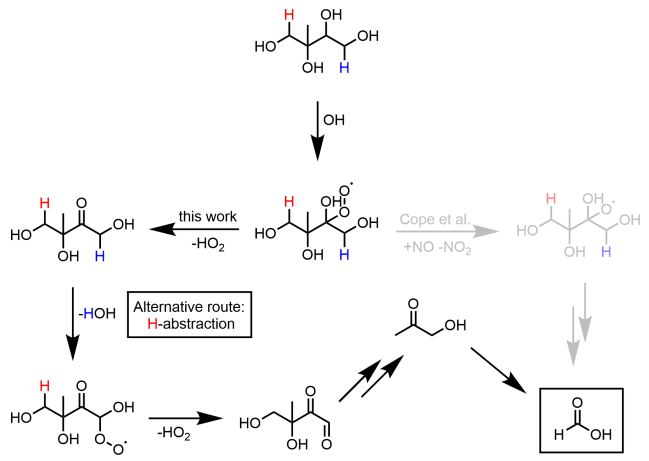

Figure 1. Simplified MeBuTETROL aqueous-phase oxidation mechanism by Cope et al. (2021) compared to the mechanism applied in MECCA. The mechanism is similarly applied for ISOPBEPX. The aqueous-phase production of formic acid happens via the oxidation of the geminal diol of methylglyoxal (not shown). The H abstraction at the red hydrogen (C_1; assumed to be 50 %) yields additional formic acid.

the formation of the geminal diol of methylglyoxal. The simplest geminal diol, from hydration of formaldehyde, has been shown to efficiently form formic acid by oxidation in both the gas and aqueous phases (Franco et al., 2021). Similarly, the geminal diol of methylglyoxal yields formic acid not only directly, but also indirectly via pyruvic acid. The related chemistry is already available in JAMOC (Rosanka et al., 2021). As an update to earlier work, we have introduced the hydrolysis of organic nitrates in the aqueous phase, formed from the gas-phase oxidation of isoprene with OH after NO addition (Vasquez et al., 2020). Similar to the small adaptation to the isoprene NO_3 mechanism, we introduce the outgassing of the oligomers of glyoxal and methylglyoxal as an update to the JAMOC mechanism. The applied H_s values can be found in Table S2 in the Supplement.

2.4 Phase partitioning

2.4.1 Henry's law solubility constants

Henry's law describes the partitioning of a compound between the gas phase and the aqueous phase. In MECCA, Henry's law solubility constant, H_s, is defined as

$$H_s = \lim_{c \to 0} c/p, \tag{1}$$

where c and p are the equilibrium concentration and partial pressure of the compound, respectively. Most values are taken from the compilation by Sander (2023). However, for many species and especially for reaction intermediates, data are not available. Therefore, an estimation method is required. Different approaches are available. The most widely used procedures are HENRYWIN and GROMHE. HENRYWIN is developed and contributed by the US Environmental Protection Agency (US-EPA, 2012). It estimates Henry's law solubility constants based on molecular structure descriptors (bond contribution) (Meylan and Howard, 1991). The training set consists of 345 species, with additional 90 chemicals for subsequent regression, and results are validated with 72 compounds. The second Henry's law solubility constant estimation method, called GROMHE, is based on a group contribution approach. Similar to HENRYWIN, the estimation is executed by multiple linear regression (Raventos-Duran et al., 2010). It uses a training set of 345 species and a validation set of 143 chemicals. Raventos-Duran et al. (2010) compared both methods and concluded that both show higher uncertainties for increasing solubilities. They revealed a large error for multifunctional compounds in HENRYWIN using the GROMHE validation set. H_s values are overestimated for difunctional molecules, while compounds with more than two functional groups are underestimated in HENRYWIN. However, running HENRYWIN with the training set of GROMHE led to increased precision of the HENRYWIN prediction.

Figure 2 displays the estimated Henry's law solubility constants by GROMHE and HENRYWIN for the closed-shell compounds of the newly implemented limonene mechanism. The diagram displays good agreement between the two methods for a vast majority of the estimations, while a small subset shows a high deviation. Of all values, 61 % lies within an order of magnitude. Larger prediction differences have a smaller impact on compounds with a generally high H_s, as these partition nearly completely to the aqueous phase in both cases. At low to medium H_s, the compounds which are higher, estimated by GROMHE, have multiple functional groups, containing mainly hydroxyl and carbonyl groups. Compounds predicted to be more soluble by HENRYWIN mostly contain nitrate groups together with further functional groups containing oxygen. A comparison to COSMOtherm values from Wang et al. (2017) does not support either of the estimation methods but lies generally in between the predictions. We use the H_s estimated by GROMHE. We chose GROMHE over HENRYWIN because it contains a larger default training set and a better performance concerning multifunctional molecules. The new H_s values were included for compounds contained in the update. Already implemented H_s values were not changed.

2.4.2 Temperature dependence

The van 't Hoff equation describes the temperature dependence of equilibrium constants based on enthalpy. We apply it to Henry's law and define the temperature dependence factor B as

$$B = \frac{\mathrm{d} \ln H_s}{\mathrm{d}(1/T)} = \frac{-\Delta_{sol} H}{R}, \tag{2}$$

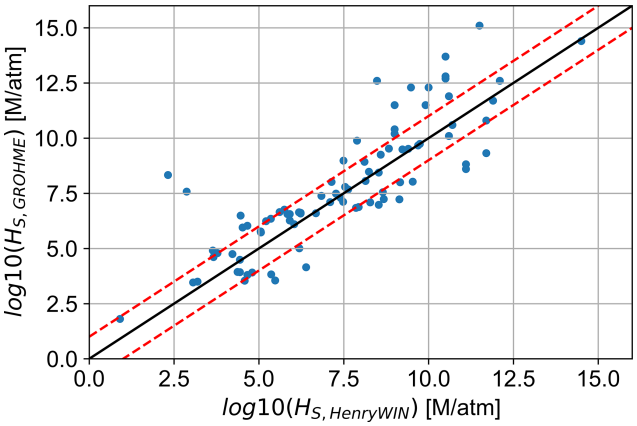

Figure 2. Comparison of H_s estimations by GROMHE and HENRYWIN for the newly implemented limonene mechanism. Both axes have a logarithmic scale. The black line represents a one-to-one comparison between both methods. The dashed red lines show a deviation of 1 order of magnitude.

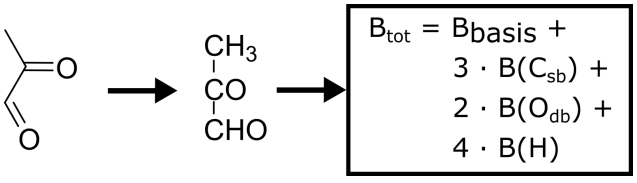

Figure 3. An example of the estimation of the temperature dependence factor B for Henry's law solubility constant of methylglyoxal. The subscript sb denotes a single and db a double bond.

where $\Delta_{sol}H$ is the enthalpy of dissolution and R is the gas constant. The substance-specific value of B is often not known, in particular for large or highly oxidized compounds. Since it can impact the partitioning considerably, it has to be estimated. Kühne et al. (2005) present an estimation approach for B based on the linear combination of B_X values for predefined molecular fragments, resulting in the final value of B. These fragments can be single atoms (e.g. carbon in the chain) or fully functional and larger groups (e.g. hydroxyl groups). Unfortunately, the hydroperoxide moiety has not been included as a molecular fragment by Kühne et al. (2005). As it plays an important role in this study, we estimate B_{OOH} to be the difference between B_{ethane} and $B_{ethylhydroperoxide}$. The B_X factors used in this study are shown in Table 2. As an example, Fig. 3 illustrates the calculation of $B_{methylglyoxal}$.

The method assumes that B_X values for different fragments are additive and that the contribution of a molecular fragment is the same for every molecule it is attached to. To compensate for this, Kühne et al. (2005) introduce correction factors for specific molecular structures that can be applied to the calculated B after estimation. The relevant correction factors for molecules included in the update are listed in Table 2. Figure 4 shows the estimated values of B compared to data found in the literature. While most molecules are predicted within 1 order of magnitude, a tendency to overpredict can be observed for some compounds. The outliers are mainly comprised of multifunctional molecules that are affected by correction factors, implying that the corrections are not strong enough to achieve fitting values. Nevertheless, this approach reflects the trend indicated by the data from Sander (2023) and Kühne et al. (2005). This estimation approach could be adjusted using additional and stronger correction factors, reflecting better the measured values. Note that B is defined differently in this work and in Kühne et al. (2005). For a direct comparison, a conversion of B is necessary (see Table 2).

Table 2. B values of group contribution and correction factors for the estimation of the temperature-dependent Henry's law solubility constants. All fragments and B values, except for the hydroperoxy fragment, are taken from Kühne et al. (2005) and converted referring to our Henry's law solubility constant definition (multiplied by ln(10)). The correction factors containing hydroxyl groups are similarly applied to hydroperoxides. The correction fragment name describes the corresponding structure in SMILES notation.

Fragment	B factor [K]
Basis	1202
C (single bond)	−60
C (double bond)	541
H	203
OH	4145
O (double bond)	2931
−O−	1966
ONO2	−811
OOH	3625
Correction factors	
C(=O)CO	−1538
COCCO	−1538
COC(OO)	−1538
C(=O)O	−3009
C(=O)OO	−3009

Figure 5 shows temperature-dependent Henry's law solubility constant, H_s, for alcohols and aldehydes between 270 and 300 K. Estimated H_s values reasonably agree with experimental values in the case of the alcohols. The aldehydes display a stronger divergence. This might be due to the hydration of the aldehydes in aqueous media or similar interactions, for which the estimation is not corrected. Nevertheless, Fig. 5 also illustrates the need for a temperature-dependent H_s, as the values of the constant vary over 1 order of magnitude. This effect is found to be more pronounced for compounds containing multiple functional groups, as more molecular fractions with high B values are applied (see Table S2). B values were added to the model for all instances of H_s without an available temperature dependency.

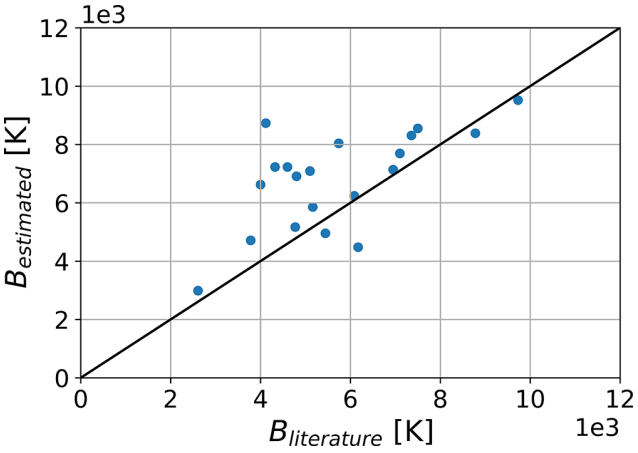

Figure 4. Comparison between the estimated and the literature temperature dependence factor B of Henry's law solubility constant. Literature data are extracted from Sander (2023) and Kühne et al. (2005).

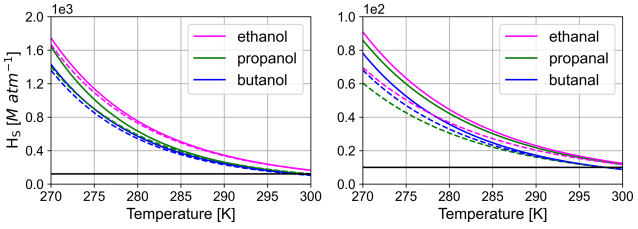

Figure 5. Comparison between estimated and experimental H_S as a function of temperature. Solid lines denote experimental and dashed lines estimated values. The solid black line denotes H_S at 298 K with no further temperature correction. Experimental data are taken from Staudinger and Roberts (2001).

3 Results and discussion

3.1 Model–model and model–observation comparison

3.1.1 Model parameters and initialization

We have evaluated the potential impacts of the new mechanism on model simulations by comparing it to the old mechanism and when modelling IEPOX observations of the Southern Oxidant and Aerosol Study (SOAS). Model conditions are adapted to conditions during the SOAS campaign. Further details of the SOAS campaign are given elsewhere (Budisulistiorini et al., 2015; Ayres et al., 2015; Sareen et al., 2016). Table 4 displays the initial mixing ratios used in all model runs in Sect. 3.1 unless mentioned otherwise. The mixing ratio of isoprene is fixed at 4 nmol mol^{-1}, which is the average measured during the SOAS campaign (Hu et al., 2015). For the same reason, the average aerosol salt content during the SOAS campaign is adopted (L. Xu et al., 2015) (see Table 3). The SOAS scenario is representative of a mildly polluted deciduous forest during summertime. All simulations are executed for a full diurnal cycle. The sensitivity runs are summarized in Table 5.

3.1.2 BASE vs. OLD run

The CAABA/MECCA box model does not simulate the production of SOA particles. Yet, a first assessment of the impact of the newly added chemistry on SOA precursors can be done by analysing low-volatility organic compounds, which can act as SOA precursors. Thus, we analyse the total (gas, aqueous, and aerosol) mixing ratios of implemented LVOCs. In the scope of this analysis, LVOCs are defined as VOCs fulfilling the condition $H_S > 10^8$ M atm^{-1}, following Hodzic et al. (2014). For evaluating the impact of the new mechanism on VOCs in different molecular size ranges, the total LVOCs have been subdivided into three groups: small LVOCs (up to four carbons), medium LVOCs (five and six carbons), and large LVOCs (more than six carbons). The new mechanism has a marginal impact on the simulated small LVOCs. Hence, this class is not included in the following discussion. Figure 6 shows the mixing ratios of the BASE and the OLD sensitivity runs at 298 and 278 K, respectively. The mixing ratios of key radicals during all sensitivity runs are depicted in the Supplement (see Figs. S10–S14).

The medium LVOCs display the largest impact. Before sunrise (prior to 08:00 on the simulated day), no substantial mixing ratios are depicted. After sunrise, mixing ratios increase for the BASE and the OLD runs, while the BASE run displays an approximately 8 times higher peak mixing ratio. This is mainly due to the formation of MeBuTETROL and organosulfates from isoprene, as shown in Fig. 7. The temperature change to 278 K lowers the medium-LVOC yield for both sensitivity runs, while the ratio between the two remains similar. For the BASE run, the concentration decrease with temperature can be explained by a decrease in IEPOX formation in the gas phase due to slower gas-phase oxidation rates (see OH mixing ratios in Fig. S13), with a simultaneous decrease in the acidity in the aqueous phase (see Fig. S15). With the main SOA pathway of IEPOX being the acid-catalysed ring opening, a lower LVOC yield is expected. Nevertheless, the ratio of IEPOX between the aqueous and gas phases increases due to a higher partitioning coefficient at low temperatures. IEPOX products increase the aerosol yield regardless of the temperature conditions. An increased production of SOA precursors from isoprene oxidation at low-NO_x conditions is expected in future global model simulations (Carlton et al., 2009; Liu et al., 2016).

The large LVOCs also increase during the full simulation period with the introduced update; however, a less pronounced change is predicted. Even though limonene and its oxidation pathways are newly introduced and show non-negligible LVOC yields, the exclusion of camphene, sabinene, and carene compensates partly for the additional LVOCs. For all three, a mechanism similar to α-pinene was assumed due to structural similarities. The oxidation of these

Table 3. Aerosol properties: chemical composition, liquid water content (LWC), and particle radius. The chemical composition is averaged from L. Xu et al. (2015). The LWC is taken from Nguyen et al. (2014). The average ambient temperature ($T_{\mathrm{ambient,SOAS}}$) and particle liquid water temperature ($T_{\mathrm{aerosol,SOAS}}$) are given to provide a better comparison between the model and observations (You et al., 2014; Nguyen et al., 2014).

Chemical composition						
NH_4^+ [$\mu g\,m^{-3}$]	NO_3^- [$\mu g\,m^{-3}$]	SO_4^{2-} [$\mu g\,m^{-3}$]	LWC [$\mu g\,m^{-3}$]	r_{aerosol} [µm]	$T_{\mathrm{ambient,SOAS}}$ [K]	$T_{\mathrm{aerosol,SOAS}}$ [K]
0.9	0.7	2.4	3.0	1.0	295.2–301.2	300.6

Table 4. Initial mixing ratios for all model runs. Values for NO and NO_2 are adapted to low, medium, and high emissions in Sect. 3.1.3. The mixing ratios of O_2, N_2, CO_2, and isoprene (C_5H_8) are fixed.

Species	Mixing ratio [nmol mol^{-1}]	Species	Mixing ratio [nmol mol^{-1}]
H_2O_2	7	methylglyoxal	0.5
O_3	25	C_5H_8	4
O_2	2.1×10^8	pan	0.1
NH_3	1	NO_3	3.15×10^{-3}
NO	2×10^{-2}	α-pinene	0.6
NO_2	4×10^{-2}	β-pinene	0.6
HNO_3	5×10^{-3}	HCOOH	0.35
N_2	7.8×10^8	limonene	0.6
CH_4	1.86×10^3	benzene	0.1
HCHO	5	acetol	4
CO	100	C_5H_{12}	0.4
CO_2	3.5×10^5	C_6H_{14}	0.4
CH_3CO_2H	2	C_7H_{16}	0.4
CH_3CO_3H	1.5	C_8H_{18}	0.4
CH_3OH	0.5	CH_3OOH	4
HONO	4×10^{-5}	toluene	0.1

Table 5. The abbreviations and descriptions of the different setups for the sensitivity runs.

Abbreviation	Description
BASE	base run with the updated mechanism
OLD	model run with CAABA/MECCA v4.5.5
BASE-278K	low-temperature run with the updated mechanism
OLD-278K	low-temperature run with CAABA/MECCA v4.5.5
High-NO_x	model run with the updated mechanism with high NO_x
Medium-NO_x	model run with the updated mechanism with medium NO_x
Low-NO_x	model run with the updated mechanism with low NO_x

monoterpenes will be reintroduced as soon as new experimental/theoretical results are accessible, including a compelling mechanism for all individual compounds. Several mechanistic studies involving camphene have been published recently (Subramani et al., 2021; Afreh et al., 2021; Li et al., 2022). Only before sunrise, when oxidation by ozone is dominant, does the OLD run outcompete the BASE run. This indicates a low LVOC yield in the mechanism of limonene and ozone for the chosen LVOC threshold. The total LVOCs show similar results to the medium LVOCs together with a positive offset of both runs due to small LVOCs. Considering the reacted VOCs and the produced LVOCs in the BASE run, we can calculate a LVOC yield to approximate the SOA yield. This analysis results in a yield of 7.3 %. With fixed isoprene concentration, it is the main LVOC contributor (approx. 90 %). Carlton et al. (2009) collected data from various studies investigating the SOA yield from isoprene and found yields of up to 6 %. Taking into account that some loss processes are not implemented yet and that the aerosol formation process is not modelled, the agreement between the model and the experiment is reasonable.

3.1.3 NO_x dependence

To estimate how anthropogenic NO_x emissions impact LVOC (and SOA) formation, we evaluate LVOC mixing ratios under varying NO_x concentrations. The main reactions of NO with peroxy radicals are O abstraction and addition, forming alkoxy radicals and nitrates, respectively. These processes compete with the formation of hydroperoxides involving HO_2. As the products from NO oxidation are generally more volatile compared to hydroperoxides, fewer LVOCs are

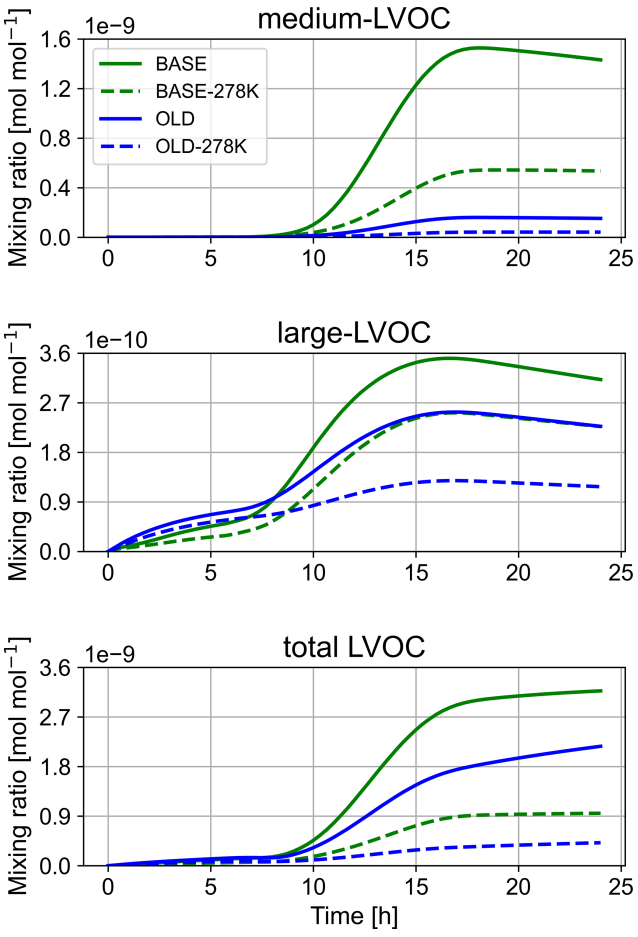

Figure 6. Temperature dependence of the LVOC formation. Results from the BASE run are shown in green, while results from the OLD run are depicted in blue. The lower-temperature runs, BASE-278K and OLD-278K, are displayed as dashed lines.

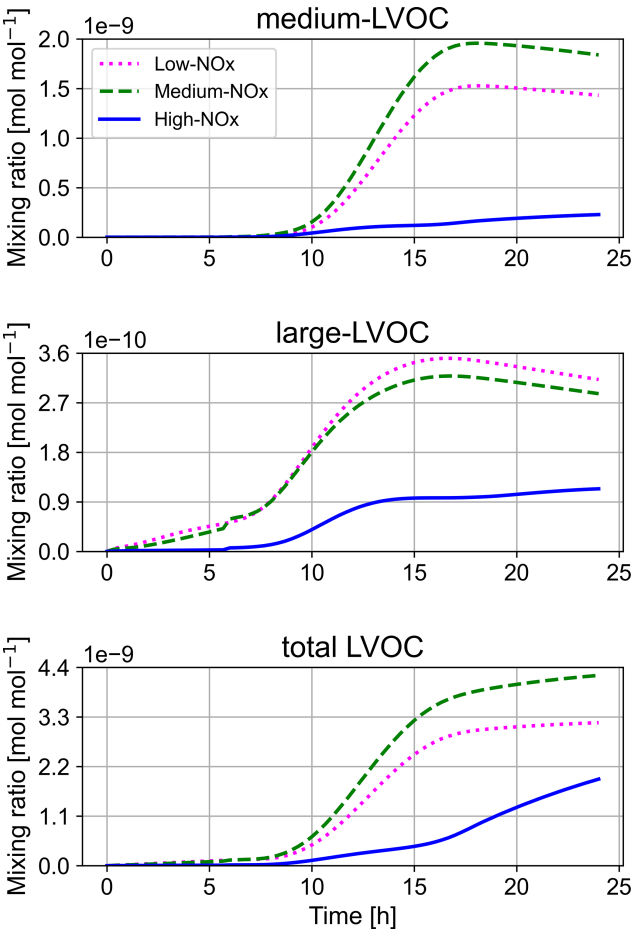

Figure 8. NO_x dependence of the LVOC formation. Results are displayed for low-NO_x (dotted magenta line), medium-NO_x (dashed green line) and high-NO_x (solid blue line) NO_x mixing ratios. For definitions of low, medium, and high, see the main text.

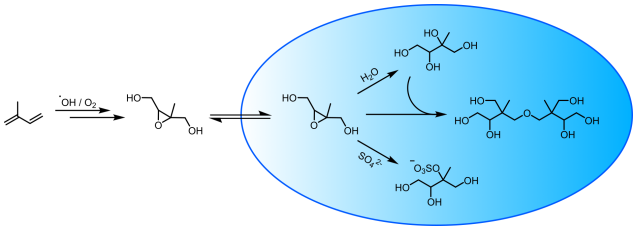

Figure 7. New aqueous-phase IEPOX scheme, leading to the formation of polyols, organosulfates, and oligomers.

formed under high-NO conditions. This hypothesis is supported by Pye et al. (2010), who estimated a low contribution of RO_2+NO reactions to the total aerosol fraction, while the RO_2+HO_2 reaction shows a higher fraction for all considered compounds (biogenic VOCs). However, this is not always the case for aromatic compounds. Based on chamber studies, J. Xu et al. (2015) found that the SOA yield and NO_x levels were correlated for toluene but anti-correlated for *m*-xylene.

Figure 8 displays the model results of the sensitivity runs for the low-, medium-, and high-NO_x scenarios. NO initial mixing ratios were set to 20 pmol mol^{-1} for modelling areas of low pollution, 2 nmol mol^{-1} for areas of medium pollution, and 20 nmol mol^{-1} for areas of high pollution. NO_2 mixing ratios are fixed to double the value of NO mixing ratios. The large LVOCs show the expected trend. With the decreasing NO_x concentration, the mixing ratios increase as a result of the higher hydroperoxide product share. Especially large-LVOC formation from ozone before sunrise is strongly NO_x-dependent. The medium LVOCs show more complex behaviour. LVOC mixing ratios rise between low and medium NO_x concentrations but fall off for high NO_x. This can be explained by the relative change in the OH concentration and the hydroperoxide yield. The OH concentration rises with increasing NO_x, while the hydroperoxide yield continuously decreases. IEPOX and many other LVOCs

require the formation of an intermediate or product hydroperoxide group. At medium NO_x levels, the rise in the OH concentration overwhelms the decreasing hydroperoxide yield for the dominant LVOC species. This trend reverses at high NO_x concentrations. Due to the comparably high total mixing ratios of the medium-LVOC bin, the total LVOC results reflect mainly the medium LVOCs.

3.1.4 Aqueous-phase chemistry

In the evaluation of the influence of temperature and NO_x on LVOCs, the aqueous oxidation of IEPOX plays a key role and increases the complexity of the reaction system. Although the box model neglects many environmental effects and dependencies, we want to compare modelled with measured mixing ratios to see whether the model produces tracer compounds in realistic amounts. For that reason, the model setup was adjusted to the conditions during the SOAS campaign (see Sect. 3.1.1). In this campaign, Hu et al. (2015) reported measurements of MeBuTETROL together with total IEPOX-SOA concentrations (combined concentrations of MeBuTETROL, C_5 triols, and isoprene-derived organic sulfates) in ambient aerosol. Assuming that the main IEPOX-SOA contributors are MeBuTETROL and the corresponding organosulfates (OSs), OS concentrations can be derived by subtracting the MeBuTETROL from the total IEPOX-SOA concentration. We extracted modelled concentrations after a full model day to compare the results. Note that this comparison is only intended to show whether the model yields results of the same order of magnitude. In measured mass concentrations, only MeBuTETROL found in aerosols is taken into account and general loss pathways are accessible (e.g. deposition). The model, on the other hand, adds up all products formed (in the gas and aqueous phases), and only the chemical loss of MeBuTETROL is considered. Wet and dry deposition and volatility-based condensation are neglected in the model runs, which is expected to result in an overprediction of LVOCs. Further, the modelled OH concentration exceeds the measurements (1.2×10^{-13} vs. 5.5×10^{-14} mol mol^{-1}; see Fig. S15 and Sanchez et al., 2018), while the pH is higher in the model (Fig. S15) than in the SOAS aerosol (Guo et al., 2015; median pH of 1). The acid-catalysed ring opening involving NO_3^- as a nucleophile, described in Eddingsaas et al. (2010), is also not considered. Thus, an overprediction by the model is expected. Table 6 displays the mean measured and modelled MeBuTETROL, OS, and total IEPOX-SOA concentrations, with and without the aqueous-phase degradation of MeBuTETROL. Modelled mass concentrations exceed the measured concentrations by an order of magnitude, while the MeBuTETROL overprediction is 50 % higher without aqueous degradation (see Fig. 1). Considering the influence factors discussed above, this assessment lends confidence that the model for IEPOX-SOA is realistic. But, it also stresses the importance of aqueous-phase degradation pathways in models. Non-negligible loss processes are still missing in the MECCA chemical scheme. The aqueous processing of all hydroperoxides, alkyl nitrates, and alkyl sulfates is not implemented, resulting in an overestimation of those species. Additionally, there is no SAR method dealing with the reactivity of epoxides towards OH radicals in aqueous media. Reaction rates have to be estimated by treating epoxides like hydroxyl groups, not considering the enthalpy gained by prompt ring opening. On the other hand, organic coatings on aqueous aerosols and the aerosol phase state may limit the reactive uptake of IEPOX and thus the production of MeBuTETROL and OS (Zhang et al., 2018; Octaviani et al., 2021).

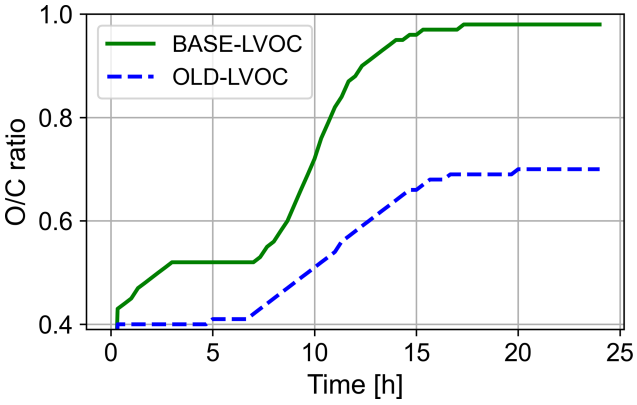

Figure 9. O / C ratio of summed up LVOCs for the BASE and OLD runs.

In addition to the LVOC concentrations, a change in the O / C ratio might occur as a result of the chemistry update. This can especially occur because LVOCs from aqueous oxidation are added, which commonly possess a higher O / C ratio (Lim et al., 2010). The main LVOC components, MeBuTETROL and OS, exhibit a ratio of 1.0 and 1.6, respectively. Thus, an increase in the O / C ratio is expected. Figure 9 displays the O / C ratio of the aqueous LVOCs for the BASE and OLD runs over the simulation time. After a full modelled day, an increase of 40 % is found, with a ratio of 0.98 and 0.70 for BASE and OLD, respectively. The updated model is in good agreement with the average O / C ratio of the SOAS campaign of 0.91 (Massoli et al., 2018). More accurate degradation pathways of MeBuTETROL and OS are expected to further improve the O / C ratio.

In addition to the already described aqSOA formation sources, there are more known but missing processes not covered by the mechanism. Formation of nitroaromatics from the aqueous-phase oxidation of anthropogenic VOCs is an important additional source of aqSOA. For instance, it has been shown that 4 % to 20 % of total SOA in Europe is aqSOA that originates from residential wood burning (Gilardoni et al., 2016). Accounting for this source of aqSOA requires the development of an explicit mechanism for heterogeneous reactions of N_2O_5 where chloride and phenols compete with water for the addition to NO_2^+ (Heal et al., 2007;

Table 6. Comparison between measured and modelled MeBuTETROL, OS, and total IEPOX-SOA mass concentrations. Measured values are taken from Hu et al. (2015). The concentrations were investigated over multiple days, but a mean concentration of 0.3 $\mu g\,m^{-3}$ is assumed in the scope of this comparison. Modelled mixing ratios are extracted after a full modelled day.

Compound	Measured [$\mu g\,m^{-3}$]	Modelled [$\mu g\,m^{-3}$]	Modelled MeBuTETROL degradation [$\mu g\,m^{-3}$]
	Hu et al. (2015)	This work	
MeBuTETROL	0.3	4.4	6.6
OS	0.6	5.3	4.4
Total IEPOX-SOA	0.9	9.7	11.0

Ryder et al., 2015; Hoffmann et al., 2018; Staudt et al., 2019). A simplified scheme for the nitration of phenol has recently been implemented into MECCA by Soni et al. (2023). Moreover, consideration of nitroaromatics during nighttime oxidation of furans from biomass burning will further increase the model predictions of SOA mass (Joo et al., 2019; Al Ali et al., 2022).

3.2 Model–chamber comparison

3.2.1 Experimental setup and considerations

Model results are compared to data from two experiments carried out in the SAPHIR (Simulation of Atmospheric PHotochemistry in a large Reaction Chamber) for further validation of the chemical mechanism. More information about the SAPHIR can be found elsewhere (Rohrer et al., 2005; Karl et al., 2006; Schlosser et al., 2007). The newly implemented limonene mechanism is tested by simulating an experiment on the ozonolysis of limonene in the dark with subsequent aerosol ageing by NO_3 (Gkatzelis et al., 2018). Thereby, the performance of the modified MCM scheme is assessed (see Sect. 2.3.2). The potential impact of the new mechanism on SOA is investigated by looking into the organic mass and the aerosol O / C ratio. The O / C ratio measured by an aerosol mass spectrometer (AMS) is used in an already corrected form, as presented in Canagaratna et al. (2015). The full mechanism in which isoprene is consumed by NO_3 (the isoprene-NO_3 mechanism) by Vereecken et al. (2021) was previously compared to the results of chamber experiments in SAPHIR (Vereecken et al., 2021). Since the mechanism included in this work is a subset of this scheme, we decided to compare it with the same chamber experiment to investigate whether using the subset gives similar results. Thus, we focus on gas-phase reactions and products. Alkyl nitrate (AN) and peroxy radical (RO_2) concentrations from model simulations based on the old and new isoprene-NO_3 mechanisms were compared to each other. RO_2 concentrations are additionally compared to measured data. For RO_2 measurements, some adjustments were applied to the model results. RO_2 radicals are not directly measured by the laser-induced fluorescence (LIF) instrument used in the campaign. To detect RO_2, they are first converted to alkoxy radicals in the reaction with NO. Formed alkoxy radicals are then expected to undergo H abstraction by O_2, yielding HO_2, which is measured by the LIF (Fuchs et al., 2008). Thus, measurement results depend on the HO_2 yield from the given alkoxy radical. For some alkoxy radicals like the methyl alkoxy radical, this yield is close to 100 % (Novelli et al., 2021; Vereecken et al., 2021). However, Novelli et al. (2021) investigated competitive reaction pathways for alkoxy radicals containing a nitrate group. In some cases, they found that decomposition (NO_2 elimination) and isomerization reactions can compete with the HO_2 production. This complicates model–experiment comparisons. To fit model results better to the RO_2 detectable by the LIF instrument, Vereecken et al. (2021) derived the subset for individual isoprene-NO_3 products that yields HO_2 (see SI of Vereecken et al., 2021). Similar to Vereecken et al. (2021) we use these values to calculate the detectable RO_2 from the total RO_2. In contrast to the mechanism by Vereecken et al. (2021) not all compounds with stereochemistry are included with all isomers in the subset scheme but are treated as lumped species. For those species, the correction for detectability is done as if the lumped species consist of 50 % of each isomer. Due to the strong dependency of the results on the NO_3 and HO_2 concentrations, model concentrations were constrained to measured data. Isoprene injections were adjusted to reproduce the observed increase in the concentration measurements of the Vocus instrument (see Brownwood et al., 2021). Vocus data were corrected by a factor of 0.7 to account for the measurements' dependency on water. Chamber injections were modelled as the increase in the injected chemical to the measured peak values within one time step. In Table 7, all injections are listed. For the limonene and isoprene experiment, dilution effects are modelled using a rate of 4.8 % h^{-1} and 5.6 % h^{-1}, respectively. Dilution rates are calculated from the mean total flow during the experiments. For the limonene experiment, this rate is applied to gas and aerosol species. The high volume-to-surface ratio of the SAPHIR minimizes the wall losses and is not considered a first approximation. Particle wall loss in particular is discussed in Sect. 3.2.2. The aerosol liquid water content (ALWC) is estimated based on AMS measurements of the high-resolution H_2O signal, which represents an approx-

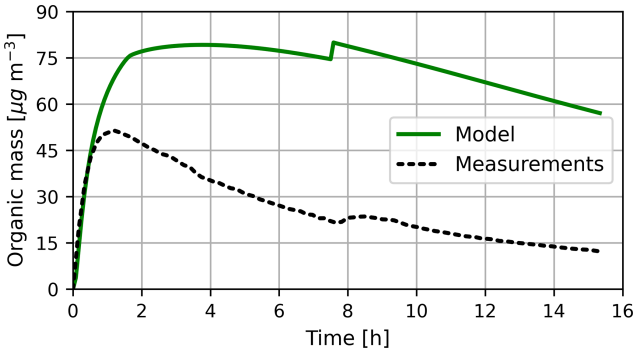

Figure 10. Mass concentration of OMC in the model and experiment. Modelled OMC represents all species with an H_s larger than 4×10^6 M atm^{-1} in either the gas phase or the aqueous phase. This simplification is applied to account for missing processes in the model. After 7.5 h, NO is injected into the chamber.

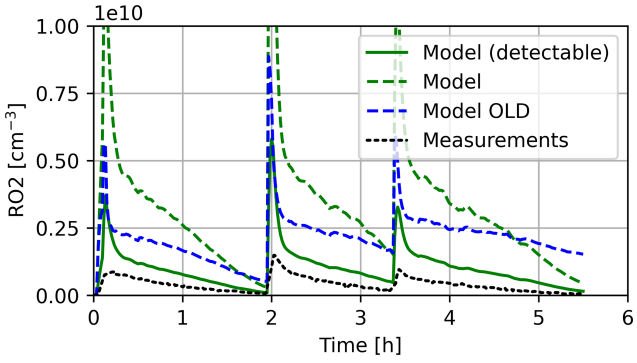

Figure 11. RO_2 mixing ratios in the model and experiment. Model results marked as detectable are modified by HO_x formation efficiencies by Vereecken et al. (2021).

imate upper limit. This signal is influenced by the interference of organics. Further information about the experiments is shown in Sect. S5 of the Supplement.

3.2.2 Limonene-ozone

The modelled and measured organic mass concentrations (OMCs) are displayed in Fig. 10. Both modelled and measured mass concentrations increase rapidly at the start of the experiment. The experimental OMC decreases after 1 h, while the model still predicts an increase. This is due to missing loss processes in the model as only the dilution of gas- and aerosol-phase species is considered although species are also lost to the chamber walls. Schmitt (2018) has shown that particle losses to chamber walls in the SAPHIR can be higher than the dilution. Figure S18 shows results for the organic mass with simplified aerosol wall loss, with a loss rate similar to Schmitt (2018). This test simulation indicates that a larger portion of the overprediction is due to missing particle loss. The nucleation and condensation of pure organics are also not modelled (see Sect. 2.2). Additionally, in the model, large compounds ($> C_4$) in the aerosol phase are currently not further oxidized (except isoprene and methylglyoxal products) (Rosanka et al., 2021), resulting in an insufficient chemical loss of organics. This missing oxidation is also reflected in the aerosol O / C ratio. In the experiment, the measured O / C ratio is in the range between 0.56 and 0.66, while the model predicts values between 0.4 and 0.51, with a similar trend (see Fig. S16). The nitrogen oxide injection after 7.5 h leads to an OMC increase in both simulation and experiment. As a result of the overall higher OMC and thus, in total, more oxidizable compounds, the model results show a steeper OMC increase after the NO injection.

The experimental data were modelled without constraining the radical concentrations to experimental values. OMC and O / C ratio values are strongly connected to the amount of limonene consumed by the different radicals (OH and ozone). As the OH concentration was not measured, the modelled OH concentration cannot be validated with experimental results. Thus, model results might be affected by incorrect radical concentrations. Figure S17 displays the OH reactivity in the model and the experiment, implying an underestimation of OH in the model.

3.2.3 Isoprene-NO_3

The modelled and measured organic peroxide radical (RO_2) mixing ratios are displayed in Fig. 11. As the new isoprene-NO_3 mechanism is an update to the previously used mechanism (in contrast to limonene), experimental results are compared to the old and new mechanism representations. The detectable RO_2 is only determined for the new mechanism, as the HO_2 yields are unknown for the RO_2 formed in the old scheme (see Sect. 3.2.1). All model simulations overpredict RO_2 concentrations, especially shortly after the VOC injections. Measured RO_2 level trends after the initial peaks show reasonable agreement between the experiment and the detectable RO_2 of the new mechanism. During times when the RO_2 concentration decreases in particular, the detectable RO_2 is in good agreement with the experimental results. The old mechanism shows an offset during times when the RO_2 concentration decreases, indicating the formation of a sufficiently stable RO_2. The RO_2 results are comparable to the simulation by Vereecken et al. (2021). Simulation results are influenced by how model variables are constrained to measured data. In Vereecken et al. (2021), constrained radical levels are fitted to experimental data, while in CAABA/MECCA, concentrations are set to the exact value measured. Thus, radical (HO_2 and NO_3) concentrations in Vereecken et al. (2021) are higher close to the injection than in the present study.

Figure 12 displays the AN mixing ratio as a function of isoprene consumed by NO_3, calculated by rate constants and concentrations from the model. Mixing ratios predicted by the new mechanism are 10 %–20 % lower than results from

Table 7. Injections used in the modelling of the chamber experiments. Model injections refer to an instantaneous change in the given mixing ratio after the previous time step.

Limonene-ozone				
Injection no.	Limonene [ppb]	Ozone [ppb]	NO [ppb]	Time since start [min]
1	23.6	140	–	0
2	–	–	30	450
Isoprene-NO_3				
Injection no.	Isoprene [ppb]	Ozone [ppb]	NO_2 [ppb]	Time since start [min]
1	–	105	24	0
2	5.1	–	–	5
3	8.0	108	23	117
4	7.0	102	25	202
5	–	111	23	360

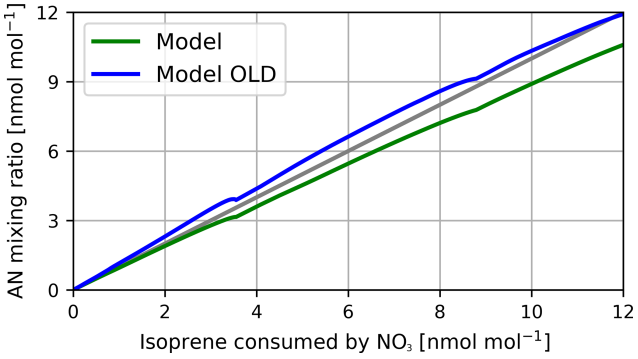

Figure 12. AN mixing ratios against isoprene consumed by NO_3. The grey line displays the 1 : 1 line.

the old scheme. Although a higher variety of AN products are accessible, in the new scheme, more loss processes are also considered. Compounds that are only lost to OH radicals in the old mechanism in particular, like 1-hydroxy-2-propanone nitrate (NOA), keep the AN concentration at high levels in the OLD run. Throughout the isoprene-NO_3 campaign, an average of 108 ± 15 % of ANs was derived, which is in reasonable agreement with the model simulations with the new mechanism (84 %–93 % AN yield). AN yields of the old mechanism are even closer to the measurements (98 %–116 % AN yield). The slight underprediction of the new model is likely due to the decomposition of organic nitrates forming small oxidized compounds and NO_2 in the degradation process. The faster AN loss processes are a potential artefact of the missing reactions from the original scheme. Nevertheless, various products in the new scheme are expected to increase the modelled SOA yield in future global simulations. Among them are functionalized epoxides and hydroperoxy nitrates.

4 Summary and outlook

We updated the chemical scheme of MECCA to improve the production of SOA precursors in the model. In addition, we investigated the partitioning from the gas to the aqueous phase of the new species formed. To assess the update, we investigated the production of LVOCs at different physical conditions and initial concentrations in a box model. As expected, we find an increase in the total mixing ratio of LVOCs, and the change in LVOCs of different sizes is also more pronounced. The results display a rising production of medium- and large-sized LVOCs, while the number of small LVOCs stays constant. This is due to the new implementation of exclusively medium to large precursors. By changing the temperature from 298 to 278 K, the model predicts a decrease in LVOC production, while an increase in SOA yield is expected. This can be attributed to the simplified way SOA is accounted for. The NO_x dependence shows more complex patterns of change. In general, the LVOC yield decreases with rising NO_x, but for medium LVOCs, an increase in moderate NO_x is found. This is due to the aqueous-phase IEPOX oxidation scheme. The modelled O / C ratio confirms the aerosol measurements of the SOAS campaign. Model simulations of chamber experiments generally aligned with experimental results, especially considering the model limitations influencing the limonene-ozone experiment. Overall, we find that the model responds differently to newly added aqueous- and gas-phase reactions. Gas-phase processes are modelled by the new mechanism well. To also better reflect the processing of VOCs and LVOCs in clouds and aerosols, more aqueous-phase reactions, for the small and large compounds as well, are needed. Furthermore, the implementation of recent findings concerning the peroxy radical reactivity might lead to additional reaction pathways or altered branching ratios (Schervish and Donahue, 2021; Mayorga et al., 2022). H shifts of peroxy radicals are only considered in the new limonene mechanism and might lead to an

increased formation of HOMs in the model if included for all compounds (Wu et al., 2021). Similarly, the treatment of peroxy radical dimerization was found to be more important than previously estimated (Schervish and Donahue, 2020). In future work, we will evaluate the impact of the new mechanism on SOA precursors with explicit multiphase kinetics in deliquescent aerosols and cloud droplets in the global model EMAC (Rosanka et al., 2024). To investigate the dependence on the results of the partitioning scheme and the Henry's law solubility constant used at a global scale, sensitivity runs will be executed with various partitioning schemes. Further, the introduction of more SOA and LVOC loss processes to the model has proven to be important, as already pointed out by Hodzic et al. (2016). A general aqueous-phase degradation scheme of organic nitrates and hydroperoxides would further refine SOA processes.

Code and data availability. The updated MECCA model code is available as a community model published under the GNU General Public License (https://www.gnu.org/copyleft/gpl.html, last access: 15 May 2024). The model code can be found in the Supplement (DOI: https://doi.org/10.5281/zenodo.10848424; Wieser, 2024) and in a code repository at https://gitlab.com/RolfSander/caaba-mecca (last access: 15 May 2024). In addition to the complete code, a list of chemical reactions including rate constants and references (meccanism.pdf) and a user manual (caaba_mecca_manual.pdf) are available in the manual directory of the Supplement. A list of all Henry's law and accommodation constants (chemprop.pdf) is available in the tools/chemprop directory. For further information and updates, the CAABA/MECCA web page at http://www.mecca.messy-interface.org (last access: 15 May 2024) can be consulted. The model data used for comparing the sensitivity runs is stored in a separate repository (https://doi.org/10.5281/zenodo.8112710, Wieser et al., 2023).

Supplement. The supplement related to this article is available online at: https://doi.org/10.5194/gmd-17-4311-2024-supplement.

Author contributions. FW and DT designed the study and developed the chemical mechanism. The latter was reviewed by all co-authors and implemented into MECCA by FW and RS. FW performed the estimation of the Henry's law coefficients. The paper was prepared by FW and reviewed by all co-authors. The measurements were carried out and analysed by CC, AN, HF, RT, and TH.

Competing interests. At least one of the (co-)authors is a member of the editorial board of *Geoscientific Model Development*. The peer-review process was guided by an independent editor, and the authors also have no other competing interests to declare.

Disclaimer. Publisher's note: Copernicus Publications remains neutral with regard to jurisdictional claims made in the text, published maps, institutional affiliations, or any other geographical representation in this paper. While Copernicus Publications makes every effort to include appropriate place names, the final responsibility lies with the authors.

Acknowledgements. The authors gratefully acknowledge the computing time granted by the Jülich Aachen Research Alliance (JARA) on the supercomputer JURECA (Jülich Supercomputing Centre, 2021) at Forschungszentrum Jülich.

Financial support. The article processing charges for this open-access publication were covered by the Forschungszentrum Jülich.

Review statement. This paper was edited by Christoph Knote and reviewed by two anonymous referees.

References

Afreh, I. K., Aumont, B., Camredon, M., and Barsanti, K. C.: Using GECKO-A to derive mechanistic understanding of secondary organic aerosol formation from the ubiquitous but understudied camphene, Atmos. Chem. Phys., 21, 11467–11487, https://doi.org/10.5194/acp-21-11467-2021, 2021.

Al Ali, F., Coeur, C., Houzel, N., Bouya, H., Tomas, A., and Romanias, M. N.: Rate Coefficients for the Gas-Phase Reactions of Nitrate Radicals with a Series of Furan Compounds, J. Phys. Chem. A, 126, 8674–8681, https://doi.org/10.1021/acs.jpca.2c03828, 2022.

Arey, J., Aschmann, S. M., Kwok, E. S. C., and Atkinson, R.: Alkyl Nitrate, Hydroxyalkyl Nitrate, and Hydroxycarbonyl Formation from the NO_x-Air Photooxidations of C_5-$-C_8$ *n*-Alkanes, J. Phys. Chem. A, 105, 1020–1027, https://doi.org/10.1021/jp003292z, 2001.

Atkinson, R., Arey, J., and Aschmann, S. M.: Atmospheric chemistry of alkanes: Review and recent developments, Atmos. Environ., 42, 5859–5871, https://doi.org/10.1016/j.atmosenv.2007.08.040, 2008.

Ayres, B. R., Allen, H. M., Draper, D. C., Brown, S. S., Wild, R. J., Jimenez, J. L., Day, D. A., Campuzano-Jost, P., Hu, W., de Gouw, J., Koss, A., Cohen, R. C., Duffey, K. C., Romer, P., Baumann, K., Edgerton, E., Takahama, S., Thornton, J. A., Lee, B. H., Lopez-Hilfiker, F. D., Mohr, C., Wennberg, P. O., Nguyen, T. B., Teng, A., Goldstein, A. H., Olson, K., and Fry, J. L.: Organic nitrate aerosol formation via NO_3+ biogenic volatile organic compounds in the southeastern United States, Atmos. Chem. Phys., 15, 13377–13392, https://doi.org/10.5194/acp-15-13377-2015, 2015.

Bates, K. H., Crounse, J. D., St. Clair, J. M., Bennett, N. B., Nguyen, T. B., Seinfeld, J. H., Stoltz, B. M., and Wennberg, P. O.: Gas phase production and loss of isoprene epoxydiols, J. Phys. Chem. A, 118, 1237–1246, https://doi.org/10.1021/jp4107958, 2014.

Brownwood, B., Turdziladze, A., Hohaus, T., Wu, R., Mentel, T. F., Carlsson, P. T., Tsiligiannis, E., Hallquist, M., Andres, S., Hantschke, L., Reimer, D., Rohrer, F., Tillmann, R., Winter, B., Liebmann, J., Brown, S. S., Kiendler-Scharr,

A., Novelli, A., Fuchs, H., and Fry, J. L.: Gas-particle partitioning and SOA yields of organonitrate products from NO_3-initiated oxidation of isoprene under varied chemical regimes, ACS Earth and Space Chemistry, 5, 785–800, https://doi.org/10.1021/acsearthspacechem.0c00311, 2021.

Budisulistiorini, S. H., Li, X., Bairai, S. T., Renfro, J., Liu, Y., Liu, Y. J., McKinney, K. A., Martin, S. T., McNeill, V. F., Pye, H. O. T., Nenes, A., Neff, M. E., Stone, E. A., Mueller, S., Knote, C., Shaw, S. L., Zhang, Z., Gold, A., and Surratt, J. D.: Examining the effects of anthropogenic emissions on isoprene-derived secondary organic aerosol formation during the 2013 Southern Oxidant and Aerosol Study (SOAS) at the Look Rock, Tennessee ground site, Atmos. Chem. Phys., 15, 8871–8888, https://doi.org/10.5194/acp-15-8871-2015, 2015.

Cabrera-Perez, D., Taraborrelli, D., Sander, R., and Pozzer, A.: Global atmospheric budget of simple monocyclic aromatic compounds, Atmos. Chem. Phys., 16, 6931–6947, https://doi.org/10.5194/acp-16-6931-2016, 2016.

Canagaratna, M. R., Jimenez, J. L., Kroll, J. H., Chen, Q., Kessler, S. H., Massoli, P., Hildebrandt Ruiz, L., Fortner, E., Williams, L. R., Wilson, K. R., Surratt, J. D., Donahue, N. M., Jayne, J. T., and Worsnop, D. R.: Elemental ratio measurements of organic compounds using aerosol mass spectrometry: characterization, improved calibration, and implications, Atmos. Chem. Phys., 15, 253–272, https://doi.org/10.5194/acp-15-253-2015, 2015.

Carlsson, P. T. M., Vereecken, L., Novelli, A., Bernard, F., Brown, S. S., Brownwood, B., Cho, C., Crowley, J. N., Dewald, P., Edwards, P. M., Friedrich, N., Fry, J. L., Hallquist, M., Hantschke, L., Hohaus, T., Kang, S., Liebmann, J., Mayhew, A. W., Mentel, T., Reimer, D., Rohrer, F., Shenolikar, J., Tillmann, R., Tsiligiannis, E., Wu, R., Wahner, A., Kiendler-Scharr, A., and Fuchs, H.: Comparison of isoprene chemical mechanisms under atmospheric night-time conditions in chamber experiments: evidence of hydroperoxy aldehydes and epoxy products from NO_3 oxidation, Atmos. Chem. Phys., 23, 3147–3180, https://doi.org/10.5194/acp-23-3147-2023, 2023.

Carlton, A. G., Turpin, B. J., Altieri, K. E., Seitzinger, S., Reff, A., Lim, H.-J., and Ervens, B.: Atmospheric oxalic acid and SOA production from glyoxal: Results of aqueous photooxidation experiments, Atmos. Environ., 41, 7588–7602, https://doi.org/10.1016/j.atmosenv.2007.05.035, 2007.

Carlton, A. G., Wiedinmyer, C., and Kroll, J. H.: A review of Secondary Organic Aerosol (SOA) formation from isoprene, Atmos. Chem. Phys., 9, 4987–5005, https://doi.org/10.5194/acp-9-4987-2009, 2009.

Carslaw, N.: A mechanistic study of limonene oxidation products and pathways following cleaning activities, Atmos. Environ., 80, 507–513, https://doi.org/10.1016/j.atmosenv.2013.08.034, 2013.

Chen, D., Zhao, Y., Zhang, J., Yu, H., and Yu, X.: Characterization and source apportionment of aerosol light scattering in a typical polluted city in the Yangtze River Delta, China, Atmos. Chem. Phys., 20, 10193–10210, https://doi.org/10.5194/acp-20-10193-2020, 2020.

Cope, J. D., Abellar, K. A., Bates, K. H., Fu, X., and Nguyen, T. B.: Aqueous photochemistry of 2-Methyltetrol and erythritol as sources of formic acid and acetic acid in the atmosphere, ACS Earth and Space Chemistry, 5, 1265–1277, https://doi.org/10.1021/acsearthspacechem.1c00107, 2021.

D'Ambro, E. L., Møller, K. H., Lopez-Hilfiker, F. D., Schobesberger, S., Liu, J., Shilling, J. E., Lee, B. H., Kjaergaard, H. G., and Thornton, J. A.: Isomerization of second-generation isoprene peroxy radicals: Epoxide formation and implications for secondary organic aerosol yields, Environ. Sci. Technol., 51, 4978–4987, https://doi.org/10.1021/acs.est.7b00460, 2017.

Eddingsaas, N. C., VanderVelde, D. G., and Wennberg, P. O.: Kinetics and products of the acid-catalyzed ring-opening of atmospherically relevant butyl epoxy alcohols, J. Phys. Chem. A, 114, 8106–8113, https://doi.org/10.1021/jp103907c, 2010.

Ehrhart, S., Dunne, E. M., Manninen, H. E., Nieminen, T., Lelieveld, J., and Pozzer, A.: Two new submodels for the Modular Earth Submodel System (MESSy): New Aerosol Nucleation (NAN) and small ions (IONS) version 1.0, Geosci. Model Dev., 11, 4987–5001, https://doi.org/10.5194/gmd-11-4987-2018, 2018.

Ervens, B.: Modeling the processing of aerosol and trace gases in clouds and fogs, Chem. Rev., 115, 4157–4198, https://doi.org/10.1021/cr5005887, 2015.

Franco, B., Blumenstock, T., Cho, C., Clarisse, L., Clerbaux, C., Coheur, P.-F., De Mazière, M., De Smedt, I., Dorn, H.-P., Emmerichs, T., Fuchs, H., Gkatzelis, G., Griffith, D. W. T., Gromov, S., Hannigan, J. W., Hase, F., Hohaus, T., Jones, N., Kerkweg, A., Kiendler-Scharr, A., Lutsch, E., Mahieu, E., Novelli, A., Ortega, I., Paton-Walsh, C., Pommier, M., Pozzer, A., Reimer, D., Rosanka, S., Sander, R., Schneider, M., Strong, K., Tillmann, R., Van Roozendael, M., Vereecken, L., Vigouroux, C., Wahner, A., and Taraborrelli, D.: Ubiquitous atmospheric production of organic acids mediated by cloud droplets, Nature, 593, 233–237, https://doi.org/10.1038/s41586-021-03462-x, 2021.

Fuchs, H., Holland, F., and Hofzumahaus, A.: Measurement of tropospheric RO_2 and HO_2 radicals by a laser-induced fluorescence instrument, Rev. Sci. Instrum., 79, 084104, https://doi.org/10.1063/1.2968712, 2008.

Gilardoni, S., Massoli, P., Paglione, M., Giulianelli, L., Carbone, C., Rinaldi, M., Decesari, S., Sandrini, S., Costabile, F., Gobbi, G. P., Pietrogrande, M. C., Visentin, M., Scotto, F., Fuzzi, S., and Facchini, M. C.: Direct observation of aqueous secondary organic aerosol from biomass-burning emissions, P. Natl. Acad. Sci. USA, 113, 10013–10018, https://doi.org/10.1073/pnas.1602212113, 2016.

Gkatzelis, G. I., Tillmann, R., Hohaus, T., Müller, M., Eichler, P., Xu, K.-M., Schlag, P., Schmitt, S. H., Wegener, R., Kaminski, M., Holzinger, R., Wisthaler, A., and Kiendler-Scharr, A.: Comparison of three aerosol chemical characterization techniques utilizing PTR-ToF-MS: a study on freshly formed and aged biogenic SOA, Atmos. Meas. Tech., 11, 1481–1500, https://doi.org/10.5194/amt-11-1481-2018, 2018.

Guo, H., Xu, L., Bougiatioti, A., Cerully, K. M., Capps, S. L., Hite Jr., J. R., Carlton, A. G., Lee, S.-H., Bergin, M. H., Ng, N. L., Nenes, A., and Weber, R. J.: Fine-particle water and pH in the southeastern United States, Atmos. Chem. Phys., 15, 5211–5228, https://doi.org/10.5194/acp-15-5211-2015, 2015.

Hallquist, M., Wenger, J. C., Baltensperger, U., Rudich, Y., Simpson, D., Claeys, M., Dommen, J., Donahue, N. M., George, C., Goldstein, A. H., Hamilton, J. F., Herrmann, H., Hoffmann, T., Iinuma, Y., Jang, M., Jenkin, M. E., Jimenez, J. L., Kiendler-Scharr, A., Maenhaut, W., McFiggans, G., Mentel, Th. F., Monod, A., Prévôt, A. S. H., Seinfeld, J. H., Surratt, J. D.,

Szmigielski, R., and Wildt, J.: The formation, properties and impact of secondary organic aerosol: current and emerging issues, Atmos. Chem. Phys., 9, 5155–5236, https://doi.org/10.5194/acp-9-5155-2009, 2009.

Heal, M. R., Harrison, M. A. J., and Neil Cape, J.: Aqueous-phase nitration of phenol by N_2O_5 and $ClNO_2$, Atmos. Environ., 41, 3515–3520, https://doi.org/10.1016/j.atmosenv.2007.02.003, 2007.

Heald, C. L., Coe, H., Jimenez, J. L., Weber, R. J., Bahreini, R., Middlebrook, A. M., Russell, L. M., Jolleys, M., Fu, T.-M., Allan, J. D., Bower, K. N., Capes, G., Crosier, J., Morgan, W. T., Robinson, N. H., Williams, P. I., Cubison, M. J., DeCarlo, P. F., and Dunlea, E. J.: Exploring the vertical profile of atmospheric organic aerosol: comparing 17 aircraft field campaigns with a global model, Atmos. Chem. Phys., 11, 12673–12696, https://doi.org/10.5194/acp-11-12673-2011, 2011.

Hens, K., Novelli, A., Martinez, M., Auld, J., Axinte, R., Bohn, B., Fischer, H., Keronen, P., Kubistin, D., Nölscher, A. C., Oswald, R., Paasonen, P., Petäjä, T., Regelin, E., Sander, R., Sinha, V., Sipilä, M., Taraborrelli, D., Tatum Ernest, C., Williams, J., Lelieveld, J., and Harder, H.: Observation and modelling of HO_x radicals in a boreal forest, Atmos. Chem. Phys., 14, 8723–8747, https://doi.org/10.5194/acp-14-8723-2014, 2014.

Herrmann, H., Schaefer, T., Tilgner, A., Styler, S. A., Weller, C., Teich, M., and Otto, T.: Tropospheric aqueous-phase chemistry: kinetics, mechanisms, and its coupling to a changing gas phase, Chem. Rev., 115, 4259–4334, https://doi.org/10.1021/cr500447k, 2015.

Hodzic, A., Aumont, B., Knote, C., Lee-Taylor, J., Madronich, S., and Tyndall, G.: Volatility dependence of Henry's law constants of condensable organics: Application to estimate depositional loss of secondary organic aerosols, Geophys. Res. Lett., 41, 4795–4804, https://doi.org/10.1002/2014GL060649, 2014.

Hodzic, A., Kasibhatla, P. S., Jo, D. S., Cappa, C. D., Jimenez, J. L., Madronich, S., and Park, R. J.: Rethinking the global secondary organic aerosol (SOA) budget: stronger production, faster removal, shorter lifetime, Atmos. Chem. Phys., 16, 7917–7941, https://doi.org/10.5194/acp-16-7917-2016, 2016.

Hoffmann, Erik, H., Tilgner, A., Wolke, R., Böge, O., Walter, A., and Herrmann, H.: Oxidation of substituted aromatic hydrocarbons in the tropospheric aqueous phase: kinetic mechanism development and modelling, Phys. Chem. Chem. Phys., 20, 10960–10977, https://doi.org/10.1039/C7CP08576A, 2018.

Hu, W. W., Campuzano-Jost, P., Palm, B. B., Day, D. A., Ortega, A. M., Hayes, P. L., Krechmer, J. E., Chen, Q., Kuwata, M., Liu, Y. J., de Sá, S. S., McKinney, K., Martin, S. T., Hu, M., Budisulistiorini, S. H., Riva, M., Surratt, J. D., St. Clair, J. M., Isaacman-Van Wertz, G., Yee, L. D., Goldstein, A. H., Carbone, S., Brito, J., Artaxo, P., de Gouw, J. A., Koss, A., Wisthaler, A., Mikoviny, T., Karl, T., Kaser, L., Jud, W., Hansel, A., Docherty, K. S., Alexander, M. L., Robinson, N. H., Coe, H., Allan, J. D., Canagaratna, M. R., Paulot, F., and Jimenez, J. L.: Characterization of a real-time tracer for isoprene epoxydiols-derived secondary organic aerosol (IEPOX-SOA) from aerosol mass spectrometer measurements, Atmos. Chem. Phys., 15, 11807–11833, https://doi.org/10.5194/acp-15-11807-2015, 2015.

Jenkin, M., Saunders, S. M., and Pilling, M. J.: The tropospheric degradation of volatile organic compounds: A protocol for mechanism development, Atmos. Environ., 31, 81–104, https://doi.org/10.1016/S1352-2310(96)00105-7, 1997.

Jöckel, P., Tost, H., Pozzer, A., Brühl, C., Buchholz, J., Ganzeveld, L., Hoor, P., Kerkweg, A., Lawrence, M. G., Sander, R., Steil, B., Stiller, G., Tanarhte, M., Taraborrelli, D., van Aardenne, J., and Lelieveld, J.: The atmospheric chemistry general circulation model ECHAM5/MESSy1: consistent simulation of ozone from the surface to the mesosphere, Atmos. Chem. Phys., 6, 5067–5104, https://doi.org/10.5194/acp-6-5067-2006, 2006.

Jöckel, P., Kerkweg, A., Pozzer, A., Sander, R., Tost, H., Riede, H., Baumgaertner, A., Gromov, S., and Kern, B.: Development cycle 2 of the Modular Earth Submodel System (MESSy2), Geosci. Model Dev., 3, 717–752, https://doi.org/10.5194/gmd-3-717-2010, 2010.

Jöckel, P., Tost, H., Pozzer, A., Kunze, M., Kirner, O., Brenninkmeijer, C. A. M., Brinkop, S., Cai, D. S., Dyroff, C., Eckstein, J., Frank, F., Garny, H., Gottschaldt, K.-D., Graf, P., Grewe, V., Kerkweg, A., Kern, B., Matthes, S., Mertens, M., Meul, S., Neumaier, M., Nützel, M., Oberländer-Hayn, S., Ruhnke, R., Runde, T., Sander, R., Scharffe, D., and Zahn, A.: Earth System Chemistry integrated Modelling (ESCiMo) with the Modular Earth Submodel System (MESSy) version 2.51, Geosci. Model Dev., 9, 1153–1200, https://doi.org/10.5194/gmd-9-1153-2016, 2016.

Joo, T., Rivera-Rios, J. C., Takeuchi, M., Alvarado, M. J., and Ng, N. L.: Secondary Organic Aerosol Formation from Reaction of 3-Methylfuran with Nitrate Radicals, ACS Earth and Space Chemistry, 3, 922–934, https://doi.org/10.1021/acsearthspacechem.9b00068, 2019.

Jülich Supercomputing Centre: JURECA: Data Centric and Booster Modules implementing the Modular Supercomputing Architecture at Jülich Supercomputing Centre, Journal of Large-Scale Research Facilities, 7, A182, https://doi.org/10.17815/jlsrf-7-182, 2021.

Kampf, C. J., Waxman, E. M., Slowik, J. G., Dommen, J., Pfaffenberger, L., Praplan, A. P., Prévôt, A. S., Baltensperger, U., Hoffmann, T., and Volkamer, R.: Effective Henry's law partitioning and the salting constant of glyoxal in aerosols containing sulfate, Environ. Sci. Technol., 47, 4236–4244, https://doi.org/10.1021/es400083d, 2013.

Karl, M., Dorn, H.-P., Holland, F., Koppmann, R., Poppe, D., Rupp, L., Schaub, A., and Wahner, A.: Product study of the reaction of OH radicals with isoprene in the atmosphere simulation chamber SAPHIR, J. Atmos. Chem., 55, 167–187, https://doi.org/10.1007/s10874-006-9034-x, 2006.

Kerkweg, A., Sander, R., Tost, H., Jöckel, P., and Lelieveld, J.: Technical Note: Simulation of detailed aerosol chemistry on the global scale using MECCA-AERO, Atmos. Chem. Phys., 7, 2973–2985, https://doi.org/10.5194/acp-7-2973-2007, 2007.

Kühne, R., Ebert, R.-U., and Schüürmann, G.: Prediction of the temperature dependency of Henry's law constant from chemical structure, Environ. Sci. Technol., 39, 6705–6711, https://doi.org/10.1021/es050527h, 2005.

Kwok, E. S. and Atkinson, R.: Estimation of hydroxyl radical reaction rate constants for gas-phase organic compounds using a structure-reactivity relationship: An update, Atmos. Environ., 29, 1685–1695, https://doi.org/10.1016/1352-2310(95)00069-B, 1995.

Li, Q., Jiang, J., Afreh, I. K., Barsanti, K. C., and Cocker III, D. R.: Secondary organic aerosol formation from camphene oxi-

dation: measurements and modeling, Atmos. Chem. Phys., 22, 3131–3147, https://doi.org/10.5194/acp-22-3131-2022, 2022.

Lim, Y. B., Tan, Y., Perri, M. J., Seitzinger, S. P., and Turpin, B. J.: Aqueous chemistry and its role in secondary organic aerosol (SOA) formation, Atmos. Chem. Phys., 10, 10521–10539, https://doi.org/10.5194/acp-10-10521-2010, 2010.

Lin, G., Sillman, S., Penner, J. E., and Ito, A.: Global modeling of SOA: the use of different mechanisms for aqueous-phase formation, Atmos. Chem. Phys., 14, 5451–5475, https://doi.org/10.5194/acp-14-5451-2014, 2014.

Lin, Y.-H., Arashiro, M., Clapp, P. W., Cui, T., Sexton, K. G., Vizuete, W., Gold, A., Jaspers, I., Fry, R. C., and Surratt, J. D.: Gene expression profiling in human lung cells exposed to isoprene-derived secondary organic aerosol, Environ. Sci. Technol., 51, 8166–8175, https://doi.org/10.1021/acs.est.7b01967, 2017.

Liu, J., D'Ambro, E. L., Lee, B. H., Lopez-Hilfiker, F. D., Zaveri, R. A., Rivera-Rios, J. C., Keutsch, F. N., Iyer, S., Kurten, T., Zhang, Z., Gold, A., Surratt, J. D., Shilling, J. E., and Thornton, J. A.: Efficient isoprene secondary organic aerosol formation from a non-IEPOX pathway, Environ. Sci. Technol., 50, 9872–9880, https://doi.org/10.1021/acs.est.6b01872, 2016.

Lopez-Hilfiker, F., Mohr, C., D'ambro, E., Lutz, A., Riedel, T., Gaston, C., Iyer, S., Zhang, Z., Gold, A., Surratt, J., Lee, B. H., Kurten, T., Hu, W. W., Jimenez, J., Hallquist, M., and Thornton, J. A.: Molecular composition and volatility of organic aerosol in the Southeastern US: implications for IEPOX derived SOA, Environ. Sci. Technol., 50, 2200–2209, https://doi.org/10.1021/acs.est.5b04769, 2016.

Mallik, C., Tomsche, L., Bourtsoukidis, E., Crowley, J. N., Derstroff, B., Fischer, H., Hafermann, S., Hüser, I., Javed, U., Keßel, S., Lelieveld, J., Martinez, M., Meusel, H., Novelli, A., Phillips, G. J., Pozzer, A., Reiffs, A., Sander, R., Taraborrelli, D., Sauvage, C., Schuladen, J., Su, H., Williams, J., and Harder, H.: Oxidation processes in the eastern Mediterranean atmosphere: evidence from the modelling of HO_x measurements over Cyprus, Atmos. Chem. Phys., 18, 10825–10847, https://doi.org/10.5194/acp-18-10825-2018, 2018.

Massoli, P., Stark, H., Canagaratna, M. R., Krechmer, J. E., Xu, L., Ng, N. L., Mauldin III, R. L., Yan, C., Kimmel, J., Misztal, P. K., Jimenez, J. L., Jayne, J. T., and Worsnop, D. R.: Ambient measurements of highly oxidized gas-phase molecules during the southern oxidant and aerosol study (SOAS) 2013, ACS Earth and Space Chemistry, 2, 653–672, https://doi.org/10.1021/acsearthspacechem.8b00028, 2018.

Mayorga, R., Xia, Y., Zhao, Z., Long, B., and Zhang, H.: Peroxy radical autoxidation and sequential oxidation in organic nitrate formation during limonene nighttime oxidation, Environ. Sci. Technol., 56, 15 337–15 346, 2022.

McDonald, B. C., de Gouw, J. A., Gilman, J. B., Jathar, S. H., Akherati, A., Cappa, C. D., Jimenez, J. L., Lee-Taylor, J., Hayes, P. L., McKeen, S. A., Cui, Y. Y., Kim, S.-W., Gentner, D. R., Isaacman-VanWertz, G., Goldstein, A. H., Harley, R. A., Frost, G. J., Roberts, J. M., Ryerson, T. B., and Trainer, M.: Volatile chemical products emerging as largest petrochemical source of urban organic emissions, Science, 359, 760–764, https://doi.org/10.1126/science.aaq0524, 2018.

Mekic, M. and Gligorovski, S.: Ionic strength effects on heterogeneous and multiphase chemistry: Clouds versus aerosol particles, Atmos. Environ., 244, 117911, https://doi.org/10.1016/j.atmosenv.2020.117911, 2021.

Meylan, W. M. and Howard, P. H.: Bond contribution method for estimating henry's law constants, Environ. Toxicol. Chem., 10, 1283–1293, https://doi.org/10.1002/etc.5620101007, 1991.

Monod, A. and Doussin, J.: Structure-activity relationship for the estimation of OH-oxidation rate constants of aliphatic organic compounds in the aqueous phase: alkanes, alcohols, organic acids and bases, Atmos. Environ., 42, 7611–7622, https://doi.org/10.1016/j.atmosenv.2008.06.005, 2008.

Mouchel-Vallon, C., Deguillaume, L., Monod, A., Perroux, H., Rose, C., Ghigo, G., Long, Y., Leriche, M., Aumont, B., Patryl, L., Armand, P., and Chaumerliac, N.: CLEPS 1.0: A new protocol for cloud aqueous phase oxidation of VOC mechanisms, Geosci. Model Dev., 10, 1339–1362, https://doi.org/10.5194/gmd-10-1339-2017, 2017.

Nguyen, T. K. V., Petters, M. D., Suda, S. R., Guo, H., Weber, R. J., and Carlton, A. G.: Trends in particle-phase liquid water during the Southern Oxidant and Aerosol Study, Atmos. Chem. Phys., 14, 10911–10930, https://doi.org/10.5194/acp-14-10911-2014, 2014.

Nölscher, A. C., Butler, T., Auld, J., Veres, P., Muñoz, A., Taraborrelli, D., Vereecken, L., Lelieveld, J., and Williams, J.: Using total OH reactivity to assess isoprene photooxidation via measurement and model, Atmos. Environ., 89, 453–463, https://doi.org/10.1016/j.atmosenv.2014.02.024, 2014.

Novelli, A., Vereecken, L., Bohn, B., Dorn, H.-P., Gkatzelis, G. I., Hofzumahaus, A., Holland, F., Reimer, D., Rohrer, F., Rosanka, S., Taraborrelli, D., Tillmann, R., Wegener, R., Yu, Z., Kiendler-Scharr, A., Wahner, A., and Fuchs, H.: Importance of isomerization reactions for OH radical regeneration from the photooxidation of isoprene investigated in the atmospheric simulation chamber SAPHIR, Atmos. Chem. Phys., 20, 3333–3355, https://doi.org/10.5194/acp-20-3333-2020, 2020.

Novelli, A., Cho, C., Fuchs, H., Hofzumahaus, A., Rohrer, F., Tillmann, R., Kiendler-Scharr, A., Wahner, A., and Vereecken, L.: Experimental and theoretical study on the impact of a nitrate group on the chemistry of alkoxy radicals, Phys. Chem. Chem. Phys., 23, 5474–5495, 2021.

Octaviani, M., Shrivastava, M., Zaveri, R. A., Zelenyuk, A., Zhang, Y., Rasool, Q. Z., Bell, D. M., Riva, M., Glasius, M., and Surratt, J. D.: Modeling the Size Distribution and Chemical Composition of Secondary Organic Aerosols during the Reactive Uptake of Isoprene-Derived Epoxydiols under Low-Humidity Condition, ACS Earth and Space Chemistry, 5, 3247–3257, https://doi.org/10.1021/acsearthspacechem.1c00303, 2021.

Pang, J. Y. S., Novelli, A., Kaminski, M., Acir, I.-H., Bohn, B., Carlsson, P. T. M., Cho, C., Dorn, H.-P., Hofzumahaus, A., Li, X., Lutz, A., Nehr, S., Reimer, D., Rohrer, F., Tillmann, R., Wegener, R., Kiendler-Scharr, A., Wahner, A., and Fuchs, H.: Investigation of the limonene photooxidation by OH at different NO concentrations in the atmospheric simulation chamber SAPHIR (Simulation of Atmospheric PHotochemistry In a large Reaction Chamber), Atmos. Chem. Phys., 22, 8497–8527, https://doi.org/10.5194/acp-22-8497-2022, 2022.

Perring, A. E., Pusede, S. E., and Cohen, R. C.: An Observational Perspective on the Atmospheric Impacts of Alkyl and Multifunctional Nitrates on Ozone and Secondary Organic Aerosol, Chem. Rev., 113, 5848–5870, https://doi.org/10.1021/cr300520x, 2013.

Petters, S. S., Cui, T., Zhang, Z., Gold, A., McNeill, V. F., Surratt, J. D., and Turpin, B. J.: Organosulfates from Dark Aqueous Reactions of Isoprene-Derived Epoxydiols Under Cloud and Fog Conditions: Kinetics, Mechanism, and Effect of Reaction Environment on Regioselectivity of Sulfate Addition, ACS Earth and Space Chemistry, 5, 474–486, https://doi.org/10.1021/acsearthspacechem.0c00293?ref=pdf, 2021.

Pozzer, A., Reifenberg, S. F., Kumar, V., Franco, B., Kohl, M., Taraborrelli, D., Gromov, S., Ehrhart, S., Jöckel, P., Sander, R., Fall, V., Rosanka, S., Karydis, V., Akritidis, D., Emmerichs, T., Crippa, M., Guizzardi, D., Kaiser, J. W., Clarisse, L., Kiendler-Scharr, A., Tost, H., and Tsimpidi, A.: Simulation of organics in the atmosphere: evaluation of EMACv2.54 with the Mainz Organic Mechanism (MOM) coupled to the ORACLE (v1.0) submodel, Geosci. Model Dev., 15, 2673–2710, https://doi.org/10.5194/gmd-15-2673-2022, 2022.

Pringle, K. J., Tost, H., Message, S., Steil, B., Giannadaki, D., Nenes, A., Fountoukis, C., Stier, P., Vignati, E., and Lelieveld, J.: Description and evaluation of GMXe: a new aerosol submodel for global simulations (v1), Geosci. Model Dev., 3, 391–412, https://doi.org/10.5194/gmd-3-391-2010, 2010.

Pye, H. O. T., Chan, A. W. H., Barkley, M. P., and Seinfeld, J. H.: Global modeling of organic aerosol: the importance of reactive nitrogen (NO_x and NO_3), Atmos. Chem. Phys., 10, 11261–11276, https://doi.org/10.5194/acp-10-11261-2010, 2010.

Raventos-Duran, T., Camredon, M., Valorso, R., Mouchel-Vallon, C., and Aumont, B.: Structure-activity relationships to estimate the effective Henry's law constants of organics of atmospheric interest, Atmos. Chem. Phys., 10, 7643–7654, https://doi.org/10.5194/acp-10-7643-2010, 2010.

Riedel, T. P., Lin, Y.-H., Zhang, Z., Chu, K., Thornton, J. A., Vizuete, W., Gold, A., and Surratt, J. D.: Constraining condensed-phase formation kinetics of secondary organic aerosol components from isoprene epoxydiols, Atmos. Chem. Phys., 16, 1245–1254, https://doi.org/10.5194/acp-16-1245-2016, 2016.

Rohrer, F., Bohn, B., Brauers, T., Brüning, D., Johnen, F.-J., Wahner, A., and Kleffmann, J.: Characterisation of the photolytic HONO-source in the atmosphere simulation chamber SAPHIR, Atmos. Chem. Phys., 5, 2189–2201, https://doi.org/10.5194/acp-5-2189-2005, 2005.

Rosanka, S., Sander, R., Wahner, A., and Taraborrelli, D.: Oxidation of low-molecular-weight organic compounds in cloud droplets: development of the Jülich Aqueous-phase Mechanism of Organic Chemistry (JAMOC) in CAABA/MECCA (version 4.5.0), Geosci. Model Dev., 14, 4103–4115, https://doi.org/10.5194/gmd-14-4103-2021, 2021.

Rosanka, S., Tost, H., Sander, R., Jöckel, P., Kerkweg, A., and Taraborrelli, D.: How non-equilibrium aerosol chemistry impacts particle acidity: the GMXe AERosol CHEMistry (GMXe–AERCHEM, v1.0) sub-submodel of MESSy, Geosci. Model Dev., 17, 2597–2615, https://doi.org/10.5194/gmd-17-2597-2024, 2024.

Ryder, O. S., Campbell, N. R., Shaloski, M., Al-Mashat, H., Nathanson, G. M., and Bertram, T. H.: Role of Organics in Regulating $ClNO_2$ Production at the Air–Sea Interface, J. Phys. Chem. A, 119, 8519–8526, https://doi.org/10.1021/jp5129673, 2015.

Sanchez, D., Jeong, D., Seco, R., Wrangham, I., Park, J.-H., Brune, W. H., Koss, A., Gilman, J., de Gouw, J., Misztal, P., Goldstein, A., Baumann, K., Wennberg, P. O., Keutsch, F. N., Guenther, A., and Kim, S.: Intercomparison of OH and OH reactivity measurements in a high isoprene and low NO environment during the Southern Oxidant and Aerosol Study (SOAS), Atmos. Environ., 174, 227–236, https://doi.org/10.1016/j.atmosenv.2017.10.056, 2018.

Sander, R.: Compilation of Henry's law constants (version 5.0.0) for water as solvent, Atmos. Chem. Phys., 23, 10901–12440, https://doi.org/10.5194/acp-23-10901-2023, 2023.

Sander, R., Kerkweg, A., Jöckel, P., and Lelieveld, J.: Technical note: The new comprehensive atmospheric chemistry module MECCA, Atmos. Chem. Phys., 5, 445–450, https://doi.org/10.5194/acp-5-445-2005, 2005.

Sander, R., Baumgaertner, A., Gromov, S., Harder, H., Jöckel, P., Kerkweg, A., Kubistin, D., Regelin, E., Riede, H., Sandu, A., Taraborrelli, D., Tost, H., and Xie, Z.-Q.: The atmospheric chemistry box model CAABA/MECCA-3.0, Geosci. Model Dev., 4, 373–380, https://doi.org/10.5194/gmd-4-373-2011, 2011.

Sander, R., Jöckel, P., Kirner, O., Kunert, A. T., Landgraf, J., and Pozzer, A.: The photolysis module JVAL-14, compatible with the MESSy standard, and the JVal PreProcessor (JVPP), Geosci. Model Dev., 7, 2653–2662, https://doi.org/10.5194/gmd-7-2653-2014, 2014.

Sander, R., Baumgaertner, A., Cabrera-Perez, D., Frank, F., Gromov, S., Grooß, J.-U., Harder, H., Huijnen, V., Jöckel, P., Karydis, V. A., Niemeyer, K. E., Pozzer, A., Riede, H., Schultz, M. G., Taraborrelli, D., and Tauer, S.: The community atmospheric chemistry box model CAABA/MECCA-4.0, Geosci. Model Dev., 12, 1365–1385, https://doi.org/10.5194/gmd-12-1365-2019, 2019.

Sareen, N., Carlton, A. G., Surratt, J. D., Gold, A., Lee, B., Lopez-Hilfiker, F. D., Mohr, C., Thornton, J. A., Zhang, Z., Lim, Y. B., and Turpin, B. J.: Identifying precursors and aqueous organic aerosol formation pathways during the SOAS campaign, Atmos. Chem. Phys., 16, 14409–14420, https://doi.org/10.5194/acp-16-14409-2016, 2016.

Schervish, M. and Donahue, N. M.: Peroxy radical chemistry and the volatility basis set, Atmos. Chem. Phys., 20, 1183–1199, https://doi.org/10.5194/acp-20-1183-2020, 2020.

Schervish, M. and Donahue, N. M.: Peroxy radical kinetics and new particle formation, Environmental Science: Atmospheres, 1, 79–92, 2021.

Schlosser, E., Bohn, B., Brauers, T., Dorn, H.-P., Fuchs, H., Häseler, R., Hofzumahaus, A., Holland, F., Rohrer, F., Rupp, L. O., Siese, M., Tillmann, R., and Wahner, A.: Intercomparison of two hydroxyl radical measurement techniques at the atmosphere simulation chamber SAPHIR, J. Atmos. Chem., 56, 187–205, https://doi.org/10.1007/s10874-006-9049-3, 2007.

Schmitt, S.: Formation of Secondary Organic Aerosol from Photo-Oxidation of Benzene: a Chamber Study, PhD thesis, Universität Bayreuth, ISBN 978-3-95806-305-1, http://hdl.handle.net/2128/18478 (last access: 15 May 2024), 2018.

Seinfeld, J. H. and Pandis, S. N.: Atmospheric chemistry and physics: from air pollution to climate change, John Wiley & Sons, ISBN 9781119221173, 2016.

Shrivastava, M., Cappa, C. D., Fan, J., Goldstein, A. H., Guenther, A. B., Jimenez, J. L., Kuang, C., Laskin, A., Martin, S. T., Ng,

N. L., Petaja, T., Pierce, J. R., Rasch, P. J., Roldin, P., Seinfeld, J. H., Shilling, J., Smith, J. N., Thornton, J. A., Volkamer, R., Wang, J., Worsnop, D. R., Zaveri, R. A., Zelenyuk, A., and Zhang, Q.: Recent advances in understanding secondary organic aerosol: Implications for global climate forcing, Rev. Geophys., 55, 509–559, https://doi.org/10.1002/2016RG000540, 2017.

Sivaramakrishnan, R. and Michael, J.: Rate constants for OH with selected large alkanes: shock-tube measurements and an improved group scheme, J. Phys. Chem. A, 113, 5047–5060, https://doi.org/10.1021/jp810987u, 2009.

Soni, M., Sander, R., Sahu, L. K., Taraborrelli, D., Liu, P., Patel, A., Girach, I. A., Pozzer, A., Gunthe, S. S., and Ojha, N.: Comprehensive multiphase chlorine chemistry in the box model CAABA/MECCA: implications for atmospheric oxidative capacity, Atmos. Chem. Phys., 23, 15165–15180, https://doi.org/10.5194/acp-23-15165-2023, 2023.

Staudinger, J. and Roberts, P. V.: A critical compilation of Henry's law constant temperature dependence relations for organic compounds in dilute aqueous solutions, Chemosphere, 44, 561–576, https://doi.org/10.1016/S0045-6535(00)00505-1, 2001.

Staudt, S., Gord, J. R., Karimova, N. V., McDuffie, E. E., Brown, S. S., Gerber, R. B., Nathanson, G. M., and Bertram, T. H.: Sulfate and Carboxylate Suppress the Formation of $ClNO_2$ at Atmospheric Interfaces, ACS Earth and Space Chemistry, 3, 1987–1997, https://doi.org/10.1021/acsearthspacechem.9b00177, 2019.

St. Clair, J. M., Rivera-Rios, J. C., Crounse, J. D., Knap, H. C., Bates, K. H., Teng, A. P., Jørgensen, S., Kjaergaard, H. G., Keutsch, F. N., and Wennberg, P. O.: Kinetics and products of the reaction of the first-generation isoprene hydroxy hydroperoxide (ISOPOOH) with OH, J. Phys. Chem. A, 120, 1441–1451, https://doi.org/10.1021/acs.jpca.5b06532, 2016.

Subramani, M., Saravanan, V., Theerthagiri, J., Subramaniam, V., Pazhanivel, T., Ramasamy, S., and Manickam, S.: Kinetics and degradation of camphene with OH radicals and its subsequent fate under the atmospheric O_2 and NO radicals – A theoretical study, Chemosphere, 267, 129250, https://doi.org/10.1016/j.chemosphere.2020.129250, 2021.

Taraborrelli, D., Lawrence, M. G., Crowley, J. N., Dillon, T. J., Gromov, S., Groß, C. B. M., Vereecken, L., and Lelieveld, J.: Hydroxyl radical buffered by isoprene oxidation over tropical forests, Nat. Geosci., 5, 190–193, https://doi.org/10.1038/ngeo1405, 2012.

Taraborrelli, D., Cabrera-Perez, D., Bacer, S., Gromov, S., Lelieveld, J., Sander, R., and Pozzer, A.: Influence of aromatics on tropospheric gas-phase composition, Atmos. Chem. Phys., 21, 2615–2636, https://doi.org/10.5194/acp-21-2615-2021, 2021.

Teng, A. P., Crounse, J. D., Lee, L., St. Clair, J. M., Cohen, R. C., and Wennberg, P. O.: Hydroxy nitrate production in the OH-initiated oxidation of alkenes, Atmos. Chem. Phys., 15, 4297–4316, https://doi.org/10.5194/acp-15-4297-2015, 2015.

Tilmes, S., Hodzic, A., Emmons, L., Mills, M., Gettelman, A., Kinnison, D. E., Park, M., Lamarque, J.-F., Vitt, F., Shrivastava, M., Campuzano-Jost, P., Jimenez, J. L., and Liu, X.: Climate forcing and trends of organic aerosols in the Community Earth System Model (CESM2), J. Adv. Model. Earth Sy., 11, 4323–4351, https://doi.org/10.1029/2019MS001827, 2019.

Tost, H., Jöckel, P., Kerkweg, A., Sander, R., and Lelieveld, J.: Technical note: A new comprehensive SCAVenging submodel for global atmospheric chemistry modelling, Atmos. Chem. Phys., 6, 565–574, https://doi.org/10.5194/acp-6-565-2006, 2006.

Tsimpidi, A. P., Karydis, V. A., Pozzer, A., Pandis, S. N., and Lelieveld, J.: ORACLE (v1.0): module to simulate the organic aerosol composition and evolution in the atmosphere, Geosci. Model Dev., 7, 3153–3172, https://doi.org/10.5194/gmd-7-3153-2014, 2014.

US-EPA: Estimation Programs Interface Suite™ for Microsoft® Windows, v 4.11, united States Environmental Protection Agency, Washington, DC, USA [software], https://www.epa.gov/tsca-screening-tools/download-epi-suitetm-estimation-program-interface-v411 (last access: 15 May 2024), 2012.

Vasquez, K. T., Crounse, J. D., Schulze, B. C., Bates, K. H., Teng, A. P., Xu, L., Allen, H. M., and Wennberg, P. O.: Rapid hydrolysis of tertiary isoprene nitrate efficiently removes NO_x from the atmosphere, P. Natl. Acad. Sci. USA, 117, 33011–33016, https://doi.org/10.1073/pnas.2017442117, 2020.

Vereecken, L.: Reaction mechanisms for the atmospheric oxidation of monocyclic aromatic compounds, in: Advances in Atmospheric Chemistry: Volume 2: Organic Oxidation and Multiphase Chemistry, World Scientific, 377–527, https://doi.org/10.1142/9789813271838_0006, 2019.

Vereecken, L. and Nozière, B.: H migration in peroxy radicals under atmospheric conditions, Atmos. Chem. Phys., 20, 7429–7458, https://doi.org/10.5194/acp-20-7429-2020, 2020.

Vereecken, L. and Peeters, J.: A theoretical study of the OH-initiated gas-phase oxidation mechanism of β-pinene ($C_{10}H_{16}$): first generation products, Phys. Chem. Chem. Phys., 14, 3802–3815, https://doi.org/10.1039/c2cp23711c, 2012.

Vereecken, L., Carlsson, P., Novelli, A., Bernard, F., Brown, S., Cho, C., Crowley, J., Fuchs, H., Mellouki, W., Reimer, D., Shenolikar, J., Tillmann, R., Zhou, L., Kiendler-Scharr, A., and Wahner, A.: Theoretical and experimental study of peroxy and alkoxy radicals in the NO_3-initiated oxidation of isoprene, Phys. Chem. Chem. Phys., 23, 5496–5515, https://doi.org/10.1039/D0CP06267G, 2021.

Wang, C., Yuan, T., Wood, S. A., Goss, K.-U., Li, J., Ying, Q., and Wania, F.: Uncertain Henry's law constants compromise equilibrium partitioning calculations of atmospheric oxidation products, Atmos. Chem. Phys., 17, 7529–7540, https://doi.org/10.5194/acp-17-7529-2017, 2017.

Wang, L., Wu, R., and Xu, C.: Atmospheric oxidation mechanism of benzene. Fates of alkoxy radical intermediates and revised mechanism, J. Phys. Chem. A, 117, 14163–14168, https://doi.org/10.1021/jp4101762, 2013.

Wennberg, P. O., Bates, K. H., Crounse, J. D., Dodson, L. G., McVay, R. C., Mertens, L. A., Nguyen, T. B., Praske, E., Schwantes, R. H., Smarte, M. D., St Clair, J. M., Teng, A. P., Zhang, X., and Seinfeld, J. H.: Gas-phase reactions of isoprene and its major oxidation products, Chem. Rev., 118, 3337–3390, https://doi.org/10.1021/acs.chemrev.7b00439, 2018.

Wieser, F.: CAABA/MECCA – SOA update – archive, Zenodo [code], https://doi.org/10.5281/zenodo.10848424, 2024.

Wieser, F., Sander, R., and Taraborrelli, D.: Model output from CAABA/MECCA study "Development of a multiphase chemical mechanism to improve secondary organic aerosol formation in CAABA/MECCA (version 4.7.0)" (1.0), Zenodo [data set], https://doi.org/10.5281/zenodo.8112710, 2023.

Wu, R., Pan, S., Li, Y., and Wang, L.: Atmospheric oxidation mechanism of toluene, J. Phys. Chem. A, 118, 4533–4547, 2014.

Wu, X., Huang, C., Chai, J., and Zhang, F.: Formation of Substituted Alkyls as Precursors of Peroxy Radicals with a Rapid H-Shift in the Atmosphere, J. Phys. Chem. Lett., 12, 8790–8797, https://doi.org/10.1021/acs.jpclett.1c02503, 2021.

Xu, J., Griffin, R. J., Liu, Y., Nakao, S., and Cocker III, D. R.: Simulated impact of NOx on SOA formation from oxidation of toluene and m-xylene, Atmos. Environ., 101, 217–225, https://doi.org/10.1016/j.atmosenv.2014.11.008, 2015.

Xu, L., Suresh, S., Guo, H., Weber, R. J., and Ng, N. L.: Aerosol characterization over the southeastern United States using high-resolution aerosol mass spectrometry: spatial and seasonal variation of aerosol composition and sources with a focus on organic nitrates, Atmos. Chem. Phys., 15, 7307–7336, https://doi.org/10.5194/acp-15-7307-2015, 2015.

Xu, L., Møller, K. H., Crounse, J. D., Kjaergaard, H. G., and Wennberg, P. O.: New insights into the radical chemistry and product distribution in the OH-initiated oxidation of benzene, Environ. Sci. Technol., 54, 13467–13477, https://doi.org/10.1021/acs.est.0c04780, 2020.

You, Y., Kanawade, V. P., de Gouw, J. A., Guenther, A. B., Madronich, S., Sierra-Hernández, M. R., Lawler, M., Smith, J. N., Takahama, S., Ruggeri, G., Koss, A., Olson, K., Baumann, K., Weber, R. J., Nenes, A., Guo, H., Edgerton, E. S., Porcelli, L., Brune, W. H., Goldstein, A. H., and Lee, S.-H.: Atmospheric amines and ammonia measured with a chemical ionization mass spectrometer (CIMS), Atmos. Chem. Phys., 14, 12181–12194, https://doi.org/10.5194/acp-14-12181-2014, 2014.

Zaytsev, A., Koss, A. R., Breitenlechner, M., Krechmer, J. E., Nihill, K. J., Lim, C. Y., Rowe, J. C., Cox, J. L., Moss, J., Roscioli, J. R., Canagaratna, M. R., Worsnop, D. R., Kroll, J. H., and Keutsch, F. N.: Mechanistic study of the formation of ring-retaining and ring-opening products from the oxidation of aromatic compounds under urban atmospheric conditions, Atmos. Chem. Phys., 19, 15117–15129, https://doi.org/10.5194/acp-19-15117-2019, 2019.

Zhang, Y., Chen, Y., Lambe, A. T., Olson, N. E., Lei, Z., Craig, R. L., Zhang, Z., Gold, A., Onasch, T. B., Jayne, J. T., Worsnop, D. R., Gaston, C. J., Thornton, J. A., Vizuete, W., Ault, A. P., and Surratt, J. D.: Effect of the Aerosol-Phase State on Secondary Organic Aerosol Formation from the Reactive Uptake of Isoprene-Derived Epoxydiols (IEPOX), Environ. Sci. Tech. Let., 5, 167–174, https://doi.org/10.1021/acs.estlett.8b00044, 2018.

Zhong, M. and Jang, M.: Light absorption coefficient measurement of SOA using a UV–Visible spectrometer connected with an integrating sphere, Atmos. Environ., 45, 4263–4271, https://doi.org/10.1016/j.atmosenv.2011.04.082, 2011.

Zhu, J., Penner, J. E., Lin, G., Zhou, C., Xu, L., and Zhuang, B.: Mechanism of SOA formation determines magnitude of radiative effects, P. Natl. Acad. Sci. USA, 114, 12685–12690, https://doi.org/10.1073/pnas.1712273114, 2017.